LIGNIN DISSOLUTION IN DEEP EUTECTIC SOLVENTS: A MOLECULAR DYNAMICS STUDY

A Thesis

presented to

the Faculty of the Graduate School

at the University of Missouri-Columbia

In Partial Fulfillment

of the Requirements for the Degree

Master of Science

by

QIANWEI LI

Dr. Caixia Wan, Thesis Supervisor

DECEMBER 2020

The undersigned, appointed by the dean of the Graduate School, have examined the thesis entitled

LIGNIN DISSOLUTION IN DEEP EUTECTIC SOLVENTS:
A MOLECULAR DYNAMICS STUDY

presented by Qianwei Li,

a candidate for the degree of Master of Science,

and hereby certify that, in their opinion, it is worthy of acceptance.

_____

Professor Caixia Wan, chair

_____

Professor Karl Hammond, member

_____

Professor Bongkosh Vardhanabhuti, member

ACKNOWLEDGMENTS

I would like to express my sincere gratitude to my advisor, Dr. Caixia Wan, for the guidance, support, and patience throughout the graduate study. Also, I very appreciate the opportunities and freedom she gave for letting me explore my research as much as I can. Without her supervision, it would be impossible for me to walk through this important journey.

I would also like to thank Drs. Karl Hammond and Bongkosh Vardhanabhuti for their time and efforts to serve on my thesis committee as well as great advice on my research and thesis.

A special Thank You goes to Drs. Yuan Dong and Tommy Sewell for their guidance on this molecular dynamic simulation work. Many thanks also go to my lab mates, my friends, and my roommate for all their help and encouragement.

Finally, I want to thank my parents for their support, encouragement, and love throughout my graduate study.

TABLE OF CONTENTS

LIST OF TABLES

Table

LIST OF FIGURES

Figure

LIGNIN DISSOLUTION IN DEEP EUTECTIC SOLVENTS: A MOLECULAR DYNAMICS SUTDY

Qianwei Li

Dr. Caixia Wan, Thesis Supervisor

ABSTRACT

Deep eutectic solvents (DESs) have shown great potential on lignocellulosic biomass pretreatment. Many DESs are capable of extracting lignin from biomass and dissolving hemicellulose while preserving most of cellulose in lignocellulosic biomass. The objective of this thesis is to understand the interaction between DESs and lignin as well as the role of DES constituents, especially hydrogen bond donor (HBD), in such interactions. DESs with choline chloride as a hydrogen bond acceptor (HBA) and polyol/ carboxylic acid as a HBD were studied for their effects on lignin dissolution behavior.

The first part of the thesis focuses on the impact of spatial charge assignment on the simulation of a DES. The results indicate that the spatial charge assignment for DES is a key factor in determining the force/interaction energy, which would further change the microscopic arrangement of HBD/HBA. In the second part of this thesis, solvent structure of DESs with choline chloride as a HBA as well as interaction with lignin were studied via molecular dynamics (MD) simulations. Three HBDs, including ethylene glycol, formic acid, and lactic acid as well as two types of lignin models (GG lignin dimer and Adler lignin) were used to gain comprehensive understanding of the local solvent molecular arrangement, the mechanism of lignin dissolution and the dissociation of lignin from cellulose. The common supramolecular complexes in DES were found to show strong correlation with the solvent hydrogen bond network and lignin dissolution.

Specially, both functional groups (hydroxyl group vs. carboxyl group) and oxygen atom number in the HBD of a DES determined its hydrogen bond networks and the strength of its interaction with lignin, which in turn largely defined the structural changes of lignin. Also, the chloride anion as well as HBD would preferentially preposition around hydroxyl groups (e.g., α-OH and γ-OH) located in the lignin linkages. Such preference implies the potential route for bond cleavage in the lignin depolymerization. Molecular interaction between lignin and a DES played a key role in dissociating lignin from cellulose. We found that the carboxylic acid DESs can detach larger part of lignin from cellulose surface, especially on the hydrophobic surface than the polyol DES. The insights gained in this study would advance the understanding of lignin dissolution at an atomistic level and provide guidance for designing effective DESs for biomass pretreatment as well as lignin extraction and valorization toward sustainable and profitable biorefinery.

CHAPTER 1

INTRODUCTION

Lignocellulosic biomass, such as agricultural residues and woody biomass, is a promising feedstock for the production of biofuels and bioproducts to replace petroleum source-based counterparts due to the renewability, abundance, and no competition with food/feed supplies (Rogner et al., 2012). The primary components of lignocellulosic biomass are cellulose, xylan and lignin and the ratio of these three major cell wall components can vary depending on plant species and maturity (Hamelinck et al., 2005). To facilitate biomass conversion for biofuel and bioproducts, biomass pretreatment is necessary to dissociate lignocellulose complex into individual components. Various pretreatment methods, such as dilute acid, alkaline, and steam explosion, have been studied for many decades (Sankaran et al., 2020). While biomass pretreatment prioritizes cellulose conversion, the usability of the resulting lignin is important for the overall economics of cellulosic biofuel production. Therefore, new pretreatment techniques are emerging for biomass fractionation concerning both cellulose digestibility and lignin valorization.

Deep eutectic solvents (DESs) were first introduced by Abbott et al. (2004) and have become promising substitutes for ILs because of their low cost, facile synthesis, biodegradability, and greenness. Some studies considered DES to be members of ILs family because an IL can also be composed of a hydrogen-bond donor (HBD) and hydrogen-bond acceptor (HBA). Typically, quaternary ammonium salts (choline chloride in most of cases) are used as HBAs, while choices for HBDs include carboxylic acids, polyols, amine, etc., of which many have low cost and are renewable and abundant. In the

context of multi-purpose biorefinery, pretreatment using DESs is emerging as a modern pretreatment technique for biomass processing especially in terms of biomass fractionation and lignin extraction/upgrading.

DESs with different combinations of HBA and HBD can possess various physicochemical properties, which further determine solvent effects on lignin dissolution from lignocellulose complex and reaction route of lignin bond cleavage. A better understanding of lignin dissolution behavior in DESs is needed in order to design the solvents for not only generating delignified, cellulose-rich biomass but also extracting high quality, property-tailorable technical lignin. To this end, we propose to investigate the interaction of DES and lignin at an atomistic level by molecular dynamics (MD) simulation. Specially, three DESs comprising choline chloride as an HBA and ethylene glycol, formic acid, or lactic acid as an HBD were selected for MD simulations. The interactions between HBA and HBD as well as between lignin–DES constituents were studied. Structural changes of lignin dimer and Adler lignin model in DESs were also characterized. Moreover, the effects of DESs on the association of cellulose-lignin bulk model were simulated by mimicking lignin dissolution from lignocellulose complex. The mechanistic insights gained from this study would provide guidance to select DES constituents and design the solvents for biomass pretreatment as well as lignin extraction and valorization.

CHAPTER 2

LITERATURE REVIEW

Lignocellulosic biomass is non-edible plant-based materials that do not compete with food and feed supplies. Cellulose and hemicellulose, as two of the main components of lignocellulosic biomass, can be converted to ethanol or other products (e.g. xylitol) via fermentation (Kumar et al., 2016; C.-G. Liu et al., 2019). However, the main challenge in the conversion of lignocellulosic biomass lies in increasing cellulose accessibility via reducing biomass recalcitrance. Biomass recalcitrance is mainly attributed to complex structures covalently bonded by biomass constituents. Various methods, such as chemical pretreatment, physical pretreatment, and biological pretreatment, have been developed to break down recalcitrant lignocellulosic matrix effectively, facilitating further conversion and upgrading of individual major cell wall components (i.e., cellulose, hemicellulose, and lignin).

2.1 Lignocellulosic Biomass

Lignocellulosic biomass mainly consists of cellulose (33–43% dry basis), xylan (8–22% dry basis) and lignin (17–30% dry basis) (Santos et al., 2019). Agricultural residues, woody biomass, and dedicated energy crops are the major sources of lignocellulosic biomass. For example, switchgrass, a type of herbaceous feedstock, is one of the most common dedicated energy crops, as it has high yield across a wide geographic range without high requirements for water and nutrients. The benefit of switchgrass to soil and water quality in marginal land is significant as well (Sanderson et al., 1996).

Cellulose is the most abundant polymer in biomass. It is a linear homopolymer of glucose, which is covalently linked via β-(1-4)-glycosidic bonds (Wyman et al., 2017).

Cellulose chains form hydrogen bonds with each other and produce both amorphous and crystalline regions. The cellulose regions can be divided into six categories (Iα, I(α+β), para-crystalline, accessible fibril surfaces, and inaccessible fibril surfaces) (Larsson et al., 1999), among which cellulose microfibrils are often shielded by lignin, while hemicellulose covalently bonds with lignin (Thakur et al., 2014). Cellulose crystallinity and inaccessible fibril surfaces of cellulose are two interrelated factors and both can directly affect enzymatic hydrolysis efficiency and ethanol production. Biomass pretreatment can change cellulose crystallinity and cellulose accessibility. For example, cellulose accessibility was improved by about 14% by dilute acid. Crystalline cellulose was found to associate with lignin more closely than amorphous cellulose (Lindner et al., 2013), which can be disrupted by biomass pretreatment, especially reducing cellulose crystallinity.

Lignin is a heterogeneous and chemically complex polymer formed by randomly free-radical polymerization primarily with some or all of three types of alcohol monomers, *p*-coumaryl, coniferyl, and sinapyl units. Units derived from those alcohol monolignols are termed *p*-hydroxyphenyl (H), guaiacyl (G), and syringyl (S), respectively (Kirk & Obst, 1988). Model lignins, such as Adler lignin (Adler, 1977) and Freudenberg lignin (Freudenberg & Neish, 1968), have been proposed to represent native lignin structure. Adler lignin is a model compound used for studying the mechanism of biomass pretreatment, as it includes all types of linkages that can be found in softwood lignin, as well as the G unit, which is usually the only aromatic subunit in softwood as well (Liu et al., 2008). Lignin properties in terms of interunit linkages, functional groups,

and subunits may vary depending botanical origins and liquid extraction techniques. These functions and applications of lignin are related to its physicochemical properties.

Interactions between lignin and cellulose and interactions between cellulose and hemicellulose have been studied for decades either through experiments or by computational methods. It is important to elucidate such interactions for improving our understanding of biomass recalcitrance. The interactions can have different effects, depending on the structure of the feedstocks and the number of covalent/noncovalent bonds between cellulose and hemicellulose as well as between hemicellulose and lignin. For example, a net attractive interaction was found between lignin monomer models and the surface of model cellulose microfibrils by molecular dynamics simulation (Houtman & Atalla, 1995). This absorption turned out to be cellulose-surface-dependent due to the different predominant interactions on different surfaces of crystalline cellulose. For natural crystalline cellulose, crystalline surfaces consist of the (100) face (a hydrophobic surface), the (110) face, (1-10) faces and the (010) face (hydrophilic surfaces). On the hydrophobic (100) face of crystalline cellulose, phenyl rings from lignin would be restricted to stay parallel to the surface, while on other faces of cellulose, weaker affinity on aromatic rings of lignin and stronger hydrogen bonding interaction were found (Besombes & Mazeau, 2005a). Lignin dimers, as well as 10-unit and 20-unit oligomers, were investigated as well, and similar absorption to cellulose surfaces was found in those cases but to a different extent (Besombes & Mazeau, 2005b). In recent years, such strong association between crystalline cellulose and lignin was further discussed and self-aggregation of lignin was also considered (Lindner et al., 2013). Moreover, the affinity of the (100) face of cellulose on binding to lignin was further proven to be stronger with

syringyl derivatives of lignin than for other two other lignin derivatives (Vermaas et al., 2019), which implies that the S/G ratio of lignin is one of the key factors in determining the recalcitrance of biomass. Vermaas et al. (2019) explained this absorption as a consequence of the tendency of lignin to reduce its contact surface with water. These results suggest that the recalcitrance of crystalline cellulose, one of the challenges for biomass pretreatment, arises from the high proportion of inaccessible cellulose fibrils and the adhesion of lignin. As computational methods advance, more complex lignin models and larger fragments of cellulose are expected to be introduced into the computational studies to have a more comprehensive understanding on biomass recalcitrance.

2.2 DES Pretreatment

Pretreatment of lignocellulosic biomass is a fundamental step to expose cellulose for further conversion and to extract lignin for further upgrading. Various pretreatment methods, such as chemical, physical, biological, and their combinations have been developed to fractionate lignocellulose complexes for further conversion. Compared to conventional pretreatment methods, deep eutectic solvent (DES) pretreatment is emerging for biomass pretreatment in terms of improving cellulose digestibility, hydrolyzing hemicellulose, and extracting valorizable lignin.

Deep eutectic solvents (DESs) were introduced as promising alternatives of ILs because they not only have analogous properties to ILs, but also are mildly or non-toxic, cheaper and biodegradable (Abbott et al., 2004; Zdanowicz et al., 2018). They are eutectic mixtures of a hydrogen bond acceptor (HBA) and hydrogen bond donor (HBD) with certain mixing ratios. Melting point of DESs is always lower than their individual

components (Smith et al., 2014). DESs can be divided into four types as shown in Table 2.1.

Table 2.1. General classification of DESs and their substituent hydrogen bond donors (HBD) and acceptors (HBA).

Type	HBD	HBA	Example	Application
I	Organic salts	Metal salts	C4minCl[b]+ $AlCl_3$	As electrolyte in Al/graphite battery[c]
II	Organic salts	Metal hydrates	Dimethylformamide + $MgCl_2.6H_2O$	Electrochemical deposition of magnesium[d]
III	Organic salts	Quaternary ammonium halides	ChCl + propionic acid	Lignin dissolution[e]
IV	Metal chlorides	Quaternary ammonium halides	ZnCl + urea	Electrodeposition of Zn-Ti alloys[f]

[a] Modified from literatures (Smith et al., 2014; Zdanowicz et al., 2018)
[b] Full name of C4minCl is 1-Butyl-3-methylimidazolium chloride
[c] (Yu et al., 2019)
[d] (Wang et al., 2013)
[e] (Soares et al., 2017)
[f] (Xu et al., 2014)

From Table 2.1, a type III DES is the only type without a metal ion included in the solvent. The most commonly used HBAs in type III DES are quaternary ammonium salts, with choline chloride (ChCl) as a typical choice. ChCl is cheap, has low toxicity, and is used mainly in animal feed (Frauenkron et al., 2012). In the rest of this chapter, DESs was referred in particular to choline chloride based DESs, unless stated otherwise. In terms of HBD, it can be a carboxylic acid, amine, polyol, or other compounds, and different combinations would lead to different performance in applications. Lignin shows greater solubility than cellulose or hemicellulose in Type III DES, , and lignin solubility varies when DESs have different combinations of HBD and HBA (Lynam et al., 2017). Lignin dissolution in DES, especially for kraft lignin (a commercial lignin produced in pulp industry), can be enhanced by adding a certain amount of water, which indicates that this solubility is hydrotropic (Soares et al., 2017). Due to their green character and

tailorable properties, type III DESs became popular in biomass fractionation (van Osch et al., 2017), polysaccharides processing (Zdanowicz et al., 2018) and lignin extraction and upgrading (Zhu Chen et al., 2020).

In general, the goal of chemical pretreatment is to improve the accessibility of cellulose by removing all or part of lignin and hemicellulose and to decrease the crystallinity of the cellulose. The structure and composition of biomass vary based on biomass source and even different parts of the plants that make up the biomass. It is a challenge to design a single solvent to fit all parts of biomass pretreatment. Therefore, tailorability is one of the most attractive properties of DESs. As shown in Table 2.2, not only different types of HBD can cause different performance of DESs on pretreatment, but also pretreatment on different types of biomass can have different efficiencies even within the same type of DES. In general, the more severe a DES pretreatment is, the higher the removal rate of lignin and xylan and the higher the cellulose conversion that can be achieved (D'Agostino et al., 2011; Li et al., 2018; Procentese et al., 2017). Microwave radiation also can accelerate the pretreatment process through increasing the length of selective lignin bonds (Muley et al., 2019), maximizing ionic characteristics, and increasing the molecular polarity of DESs (Liu et al., 2017). Secondly, the types and numbers of functional groups on the HBD determines the properties of particular DESs and the energy requirements during pretreatment. Carboxyl groups on carboxylic-acid–based HBDs can extract more lignin than hydroxyl groups on alcohol-based HBDs (Hou et al., 2018). Thirdly, the chain length and size of HBDs also impact the pretreatment performance. Hou et al. (2018) reported that longer alkyl chain diols did better extracting lignin than shorter alkyl chain glycols. However, Liu et al. (2017) found that HBDs with

short chains provided solutes with more opportunities to get into the free volume of solvents according to the hole theory. Fourthly, the preference of DES components to interact with solutes is based on the formation of a hydrogen bond network. Chloride ion, as a strong HBA in both DES pretreatment and IL pretreatment, disrupts the intramolecular hydrogen-bond network of lignin and cellulose (Li et al., 2018; Remsing et al., 2006). With the help of chloride ions, it is easier for the HBD to access and attack certain sites in biomass. Last but not least, the favorable interaction of DESs with lignin, which is reflected in the lignin extraction efficiencies in Table 2.2, is considered in part to be a consequence of the binding of choline chloride with the phenolic groups of lignin (Alvarez-Vasco et al., 2016).

Table 2.2. Studies of biomass pretreatment by different types of DESs.

DES	Molar ratio	Biomass	Condition	Cellulose removal [a] (wt%)	Lignin removal [b] (wt%)	Cellulose digestibility	Reference
ChCl/ethylene glycol	1:2	Potato peels	60℃, 3h	5.69	20.74	Enzymatic glucose yield: 0.12 g glucose/g glucan	(Procentese et al., 2018)
	1:1	Rice straw	80℃, 6h	15.8	21.89	23.9% glucose yield	(Hou et al., 2018)
	1:2	Potato peels	115℃, 3h	NG[c]	39.05	Enzymatic glucose yield: 0.41 g glucose/g glucan	(Procentese et al., 2018)
	1:1	Rice straw	120℃, 3h	19.39	28.7	33.2% glucose yield	(Hou et al., 2018)
	1:2	Switchgrass	130℃, 0.5h	<5	24	11% glucose yield	(Chen et al., 2018a)
	1:2	Potato peels	150℃, 3h	16.93	63.8	Enzymatic glucose yield: 0.74 g glucose/g glucan	(Procentese et al., 2018)
ChCl/glycolic acid	1:1	Rice straw	80℃, 6h	12.77	33.17	40.1% glucose yield	(Hou et al., 2018)
	1:1	Rice straw	120℃, 3h	6.26	36.88	79.1% glucose yield	(Hou et al., 2018)
ChCl/oxalic acid	1:1	Rice straw	80℃, 6h	9.97	36.8	68.3% glucose yield	(Hou et al., 2018)
	1:1	Rice straw	120℃, 3h	10.67	9.27	83.9% glucose yield	(Hou et al., 2018)
ChCl/malonic acid	1:1	Rice straw	80℃, 6h	10.15	51.29	67.4% glucose yield	(Hou et al., 2018)
ChCl/lactic acid	1:5	Rice straw	60℃, 12h	NG	59.89	36.0% saccharification	(Kumar et al., 2016)
	1:1	Rice straw	90℃, 6h, 10%(wt) H_2O	7.83	48.22	49.6% glucose yield	(Li et al., 2018)
	1:3	Rice straw	90℃, 6h, 10%(wt) H_2O	11.1	62.47	71.8% glucose yield	(Li et al., 2018)
	1:1	Rice straw	120℃, 3h, 10%(wt) H_2O	17.14	64.75	80.5% glucose yield	(Li et al., 2018)
	1:3	Rice straw	120℃, 3h, 10%(wt) H_2O	18.36	73.2	80.5% glucose yield	(Li et al., 2018)
	1:2	Switchgrass	130℃, 0.5h	2.1	83.4	86.2% glucose yield	(Zhu Chen et al., 2020)
ChCl/glycerol	1:2	Potato peels	60℃, 3h	1.88	21.04	Enzymatic glucose yield: 0.16 g glucose/g glucan	(Procentese et al., 2018)
	1:2	Lettuce	80℃, 6h	3.07	35.03	Enzymatic hydrolysis rate: 0.55 g/L h-1	(Procentese et al., 2017)
	1:2	Corn cob	80℃, 15h	12.3	20.53	Enzymatic glucose yield: 0.40 g glucose/g glucan	(Procentese et al., 2015)
	1:2	Switchgrass	110℃, 1h	0.08	17.72	11.83% glucose yield	(Chen et al., 2018c)
	1:2	Potato peels	115℃, 3h	NG	37.99	Enzymatic glucose yield: 0.48 g glucose/g glucan	(Procentese et al., 2018)
	1:2	Corn cob	115℃, 15h	6.96	26.25	Enzymatic glucose yield: 0.79 g glucose/g glucan	(Procentese et al., 2018)
	1:2	Lettuce	115℃, 16h	3.07	48.59	Enzymatic hydrolysis rate: 1.6 g/L h-1	(Procentese et al., 2017)
	1:2	Potato peels	150℃, 3h	13.61	64.75	Enzymatic glucose yield: 0.80 g glucose/g glucan	(Procentese et al., 2018)
	1:2	Corn cob	150℃, 15h	7.98	58.99	Enzymatic glucose yield: 0.91 g glucose/g glucan	(Procentese et al., 2015)
	1:2	Lettuce	150℃, 16h	7.92	72.67	Enzymatic hydrolysis rate: 2.5 g/L h-1	(Procentese et al., 2017)
ChCl/formic acid	1:1.5	Xylose residue	120℃, 2h	20	63.5	86.1% glucose yield	(Guo et al., 2018)

[a] Cellulose removal rate = $\frac{W_{untreated\ biomass} \times CC_{untreated} - W_{treated\ biomass} \times CC_{treated})}{W_{untreated\ biomass} \times CC_{untreated}} \times 100\%$, where CC stands for the composition of cellulose in percentage.

[b] Lignin removal rate = $\frac{W_{untreated\ biomass} \times CL_{untreated} - W_{treated\ biomass} \times CL_{treated})}{W_{untreated\ biomass} \times CL_{untreated}} \times 100\%$, where CL stands for the composition of lignin in percentage.

[c] NG: Negative values reported most likely due to some experimental errors.

Table 2.3. Properties of extracted lignin by DES pretreatment.

DES	Molar ratio	Biomass	Condition	Lignin solubility (%)[c]	Properties of extracted lignin[a,b,d]	Reference
ChCl/oxalic acid	1:1	Poplar wood flour	80°C, 3min; microwave	\	M_w = 913, PDI=1.25; S/G ratio=0.69 (1.41)	(Liu et al., 2017)
	1:1	Pinewood sawdust	130°C, 15min; microwave	~81	M_w = 2373, PDI = 11.41	(Muley et al., 2019)
ChCl/lactic acid	1:1	Oil palm empty fruit bunch	120°C, 8h	33.5	Total phenol hydroxyl = 3.72 mmol/g	(Tan et al., 2019)
	1:15	Oil palm empty fruit bunch	120°C, 8h	61	Total phenol hydroxyl = 3.33 mmol/g	(Tan et al., 2019)
	1:10	Willow	120°C, 12h	91.8	Purity = 94.46%, S/G ratio = 1.82; Total phenol hydroxyl = 0.915 mmol/g	(Li et al., 2017)
	1:10	Willow	120°C, 12h	\	Purity = 94.46%, Mw = 1261.1 (3324.9), PDI = 1.18 (1.24); Particle size = 494.2nm, total phenol hydroxyl = 2.05 mmol/g	(Lyu et al., 2018)
	1:9	Poplar wood meal	130°C, 6h	61.5	Purity = 95%, syringaldehyde/vanillin = 1.85; Ferulate is hardly detected	(Y. Chen et al., 2019)
ChCl/malic acid	1:1	Oil palm empty fruit bunch	120°C, 8h	22.9	Total phenol hydroxyl = 2.91 mmol/g	(Tan et al., 2019)
ChCl/formic acid	1:1.5	Xylose residue	120°C, 2h	\	M_w = 830 (6120), PDI = 1.43 (1.49)	(Guo et al., 2018)
	1:2	Oil palm empty fruit bunch	120°C, 8h	62	Total phenol hydroxyl = 2.66 mmol/g	(Tan et al., 2019)
	1:2	Pinewood sawdust	150°C, 15min; microwave	~90	M_w = 5691, PDI = 3.45	(Muley et al., 2019)
ChCl/acetic acid	1:2	Oil palm empty fruit bunch	120°C, 8h	~28	Total phenol hydroxyl = 3.25 mmol/g	(Tan et al., 2019)
ChCl/ethylene glycol	1:2	Switchgrass	130°C, 0.5h; 1wt% H_2SO_4, 10wt% H_2O	57.63	Purity = 83.16%, content of ferulate = 5.46%; M_w = 4599.5 (9544.5), PDI = 3.75 (4.89); Content of β-O-4 = 4.98% (46.72%)	(Chen et al., 2018a)
ChCl/glycerol/ $AlCl_3 \cdot 6H_2O$	1:2:0.28	Poplar wood	120°C, 4h	95.46	Purity = 94%, total phenol hydroxyl = 1.583 mmol/g; Mw = 5466, PDI = 1.67	(Xia et al., 2018)
ChCl/glycerol/ $FeCl_6$	62:124:1	Hybrid pennisetum	120°C, 6h	49	Mw = 2035 (6790), PDI = 1.96 (1.81), purity=94.5%; Content of β-O-4 = 2.3% (53.24%); Total phenol hydroxyl = 2.35 mmol/g; IC50 for antioxidant activity = 0.085 mg/ml	(Wang et al., 2019)

[a]: Mw stands for weight-average molecular weight.
[b]: PDI stands for polydispersity, which is the ratio of the weight-average molecular weight and the number-average molecular weight.
[c]: Lignin solubility was calculated based on initial amount of lignin in biomass.
[d]: Values in parentheses are the results for the native lignin.

In recent years, besides being developed to improve the cellulose accessibility for better ethanol production, biomass pretreatment is expected to achieve full utilization of biomass, which means that this process can well separate some major components of biomass, and fractioned components can be recovered and refined for multi-purposes. Lignin as the major removed component, has many potential applications, such as energy production, nanoparticles, or biodegradable polymer (Chio et al., 2019). Therefore, lignin removed from pretreatment is recovered and further studied on its properties. Because DES pretreatment not only cleaves bonds between hemicellulose and lignin but also fractionates lignin, extraction lignin (also referred to DES lignin) would possess partially-preserved characteristics of native lignin. Meanwhile, lignin self-aggregation occurs during pretreatment. Therefore, the properties of DES lignin vary depending on the severity of pretreatment and types of DESs, some of which are shown in Table 2.3. Some of those properties include purity, aromatic hydroxyl content, ratio of S to G units, molecular weight, dispersity, and abundance of β-O-4 linkages.

β-O-4 linkages are the primary type of linkage in lignin and are the most vulnerable to cleavage during pretreatment due to low association energy. Different composition of β-O-4 linkages in lignin can lead to various properties and applications of lignin. Preservation of β-O-4 linkages in DES-treated lignin is beneficial to aromatic monomer production via subsequent catalytic depolymerization, while DES-treated lignin with fewer β-O-4 linkages is thermally stable (Chen et al., 2018b). Similar to other pretreatment, β-O-4 linkages can be easily cleaved during DES pretreatment, especially at high temperature or acidic condition. Due to the cleavage of β-O-4 linkages, an increase in the total amount of aromatic hydroxyl groups (Wang et al., 2019) and occurrence of Hibbert's ketone (HK) linkages (Y. Chen et al., 2019) are observed in

DES lignin. More aromatic hydroxyl groups in lignin can improve the antioxidant and antimicrobial abilities of lignin (García et al., 2010; Wang et al., 2019).

For the change of S/G ratio, increases and decreases of this ratio were reported in different studies due to the self-aggregation behavior among guaiacyl units of lignin (Wang et al., 2019) and the demethoxy effect of DES (Liu et al., 2017), respectively. It is reasonable to infer that the self-aggregation and demethoxylation effects occur at the same time, and the properties of the DES and the severity of condition determine which effect is predominant during pretreatment. Furthermore, purity, molecular weight, and dispersity are also important, as they determine the compatibility of fractionated lignin for being used to produce other value-added products (Y. Chen et al., 2019; Guo et al., 2018).

2.3 Molecular Dynamics of DESs

In order to understand better the properties of DESs, computational methods have been used to investigate the microscopic structure of DESs in recent years. Computational methods create a connection between the microscopic structure and interaction of DES with solutes and the macroscopic details, such as thermodynamic and transport properties. For bulk phase properties, molecular dynamics (MD) simulation is a suitable tool, as it can include anywhere from several thousand to millions or even billions of atoms (Hammond et al., 2019) in one simulation. Properties calculated by MD should be compared with experimental data to make sure that the simulation is solid enough to represent the characteristics of DESs. Force field, molecular geometry, and charges of atoms determine the accuracy of the models used in the simulation. To ensure the reliability of potential energy calculation, selection of a force field is a key factor to start a good molecular simulation as it defines the potential energy and provides sets of parameters to define charges, bonds, angles, dihedrals, and electronic forces for all atoms in

simulation. In Table 2.4, some common choices of force fields and their prediction of density are listed.

Table 2.4. Common force fields used in choline chloride-based DES simulations.

Force field	Simulation software	HBD	Modification	Remark	Reference
MMFF[a]	GROMACS 4.6.5	Urea	Full charges from the force field were used for DES	Error for density at 298 K is around 1%	(Shah & Mjalli, 2014)
GAFF[b,d]	Amber 10 and 12	Urea, malic acid, glycerol	Full charges from the force field were scaled by 0.9	Standard deviations for density at temperature range from 298 K to 330K is from 5.7×10^{-5} to 1.1×10^{-5} g/cm^3	(Perkins et al., 2014)
GAFF, MMFF	GROMACS 5.1	Levulinic acid, glycerol, 1,4-Butanediol	Full charges from MMFF and charges from GAFF scaled by 0.75 were used	Deviation is less than 3% at 293 K	(Mainberger et al., 2017)
OPLS-AA[c]	GROMACS 5.0.7	Ethylene glycol, glycerol, levulinic acid, malonic acid, oxalic acid, phenol, urea	Charges from OPLS-AA were scaled by 0.8	Errors were in range from 0.1 to 4.2 at temperature from 298.15 K to 333.15 K. Overall mean absolute errors are around 1.1% to 1.3%	(Doherty & Acevedo, 2018)
OPLS-AA/AMBER	GROMACS 4.0.5	Water	Charges were scaled by 0.9	Error for density at 298 K is 3.82%	(Sun et al., 2013)
ATB[e] 2.1 server	GROMACS 5.0.6	Urea, ethylene glycol, glycerol	Full charges from the force field were used for DES	Error for density are within 5% at 303.15 K	(Zhekenov et al., 2017)

[a] MMFF: Merck molecular force field.
[b] GAFF: General AMBER force field.
[c] OPLS-AA: All-atom optimized potentials for liquid simulations.
[d] Charges for GAFF were obtained by the restrained electrostatic potential (RESP) charge derivation method.
[e] ATB: Automated Topology Builder.

A brief introduction to define force field in Table 2.4 and the corresponding potential energy calculation formulas are presented below.

The general AMBER force field (GAFF) (Wang et al., 2004) is a non-polarizable force field used for organic solvents, whose functional form is

$$E_{\text{pair}} = \sum_{\text{bonds}} K_r\,(r - r_{eq})^2 + \sum_{\text{angles}} K_\theta\,(\theta - \theta_{eq})^2 + \\ + \sum_{\text{dihedrals}} \frac{V_n}{2}[1 + \cos(n\phi - \gamma)] + \sum_{i<j}[\frac{A_{ij}}{R_{ij}^{12}} - \frac{B_{ij}}{R_{ij}^{6}} + \frac{q_i q_j}{\varepsilon R_{ij}}] \qquad (2.1)$$

where r_{eq} and q_{eq} are equilibrium structural parameters; K_r, K_q, V_n are force constants; n is the multiplicity and γ is a phase angle for torsional angle parameters.

The merck molecular force field (MMFF) (Halgren, 1996) is a force field intended for use in organic and pharmaceutical applications, whose functional form is

$$E_{\text{MMFF}} = \sum_{\text{bonds}} K_r\,(r - r_{\text{eq}})^2 \times (1 + cs(r - r_{\text{eq}}) + \frac{7}{12}cs^2(r - r_{\text{eq}})^2) \\ + \sum_{\text{angles}} K_\theta\,(\theta - \theta_{\text{eq}})^2(1 + cb(\theta - \theta_{\text{eq}})) \\ + \sum_{\text{dihedrals}} 0.5\,(V_1(1 + \cos\Phi) + V_2(1 - \cos 2\Phi) + V_3(1 + \cos 3\Phi)) \\ + \sum_{i<j} \varepsilon_{ij}\left(\frac{A_{ij}}{R_{ij} + B_{ij}}\right)^7\left(\frac{C_{ij}^7}{R_{ij}^7 + D_{ij}} - 2\right) + \sum_{i<j} \frac{q_i q_j}{[D(R_{ij} + \delta)]^n} \qquad (2.2)$$

The all-atom optimized potentials for liquid simulations (OPLS-AA) (Jorgensen et al., 1996) is a popular force field for organic molecules and peptides.

$$E_{\mathrm{OPLSAA}} = \sum_{\mathrm{bonds}} K_r\,(r - r_{eq})^2 + \sum_{\mathrm{angles}} K_\theta\,(\theta - \theta_{eq})^2 + \sum_{\mathrm{torsion}} 0.5\,(V_1(1 + \cos(\phi + f1)) + V_2(1 - \cos(2\phi + f2)) + V_3(1 + \cos(3\phi + f3))) + \sum_{i<j} \left[\frac{q_i q_j e^2}{r_{ij}} + 4\varepsilon_{ij}\left(\frac{\sigma_{ij}^{12}}{r_{ij}^{12}} - \frac{\sigma_{ij}^{6}}{r_{ij}^{6}}\right)\right] f_{ij} \quad (2.3)$$

One of the commonalities of these force fields is that they are all non-polarizable force fields designed for the simulation of pharmaceutical molecules. Although Table 2.4 only lists the density prediction for each force field, other thermodynamic properties including viscosity (Doherty & Acevedo, 2018), heat capacity (Doherty & Acevedo, 2018; Mainberger et al., 2017; Perkins et al., 2013) and self-diffusion coefficients (Doherty & Acevedo, 2018; Mainberger et al., 2017; Perkins et al., 2013; Shah & Mjalli, 2014; Zhekenov et al., 2017) are also important to check the accuracy of force field, and the accuracy in simulation varies depending on the properties and the type of DES.

It should be noted that the charge-scaling strategy is usually applied on the partial charges for atoms of DESs, due to the electron density transfer from anion to both cation and organic compound (Zahn et al., 2016). Zahn et al. (2016) also pointed out that a hydrogen bond network has strong association with the charge delocalization of DES, based on the finding that if hydrogen bonding between the chloride anion and organic compound is stronger, more charges would be transferred to HBD and thus the anion charge would become less negative. Several approaches can be employed to determine suitable partial charges for DES, for example, density functional theory (DFT)

calculations can be performed on either clusters of DES molecules or isolated molecules of DES and then charge assignment methods such as Hirshfeld-I partial charge analysis (Zahn et al., 2016), Mulliken, ChelpG, or Merz-Kollman (García et al., 2015) could be used to obtained partial charges. The other approach can be charge-scaling with scaling factor of around 0.75 to 0.9 (Doherty & Acevedo, 2018). This method uses the spatial charges for DES molecules provided by the force field of choice, then those spatial charges would be scaled so that the impact of charge delocalization of DES on molecular interaction can be also included in the simulation. However, exacting values of partial charges for DES or how the charge delocalization would affect the solvent properties remain unclear. Besides, simulation software, settings in a simulation, and ways to optimize the initial geometries of molecules also have impacts on the accuracy of a simulation on the physical and chemical properties of DESs.

Structures of some common DESs have been studied by MD simulation and some of those results have been proven to be in good agreement with experimental data from neutron diffraction (Hammond et al., 2016). The structure of DESs is determined by the dynamics interactions among three components (HBD, choline cation and chloride anion), and these interactions can be categorized into six pairs when only a neat DES is studied: choline–chloride, choline–HBD, chloride–HBD, choline–choline, chloride–chloride, and HBD–HBD. As discussed in section 2.2, the type and the number of functional groups, as well as the chain length of the HBD, can result in different efficiencies in biomass pretreatment. With the help of MD simulations, these differences can be further explored.

To thoroughly analyze the data from simulations, calculations, including center-of-mass radial distribution function (com-RDF), site–site radial distribution function (ss-

RDF), number of hydrogen bonds, and so on would be conducted, and the solvation shell of DES and the orientation of those components can be clearly illustrated. The organic compound acting as a HBD in DES usually contributes its oxygen atom(s) as HBD site(s), and these donating sites from the HBD have preference for the hydrogen bonds-accepting sites. For example, glycerol, ethylene glycol, malonic acid and oxalic acid (Gilmore et al., 2018; Perkins et al., 2014) have the strongest hydrogen bonding interaction with chloride anion, while urea shows the strongest hydrogen bonds with other urea molecules. The intensity of the interactions between the HBD and the chloride anion can be affected by the size and functional group of the HBD, the simulation temperature, and the partial charges used in simulation. At the same time, if the HBD has more than one symmetrically inequivalent donating site, different sites would have different intensities on the interaction with chloride anion, and this would affect the interaction with choline cation when the oxygen from the HBD acts more as a HBA (Mainberger et al., 2017). The behavior of HBDs becomes a driving force to form the unique structure of DES because it would complement the charge delocalization through hydrogen bonding interactions, and further realize the locally stoichiometric and charge balance due to its electric neutrality (Hammond et al., 2016).

Choline cation has relatively weak interactions with HBD, but the intensions of interactions with the anion are strong via hydrogen bonding between the hydroxyl group of choline and chloride anion (Gilmore et al., 2018). The polarity, viscosity, and self-diffusion coefficients of different DESs are influenced by the interactions among three components. Perkins et al. (2014) found that the number of hydrogen bonds at higher hydrogen bond percent occupancies have a positive correlation with viscosity based on

the same trend as ChCl/ethylene glycol < ChCl/glycerol < ChCl/urea < ChCl/malonic acid for both hydrogen bond percent occupancies and viscosities.

Besides investigating the formation and solvent structure of DESs and its corresponding physical properties, studies on interactions between DESs and solutes of interest are also interesting and important. Questions such as how DESs dissolve lignin and cellulose under different conditions or how DESs interrupt the linkages between either lignin and cellulose or hemicellulose and cellulose are expected to be elucidated. Although only a handful of studies are related to those questions and the types of computational methods used in these studies are limited, those questions have been gradually brought to the forefront in the past several years.

In some earlier studies, DFT calculations and MD simulations were performed to reveal the mechanisms of lignin/cellulose dissolution by ILs. Hydrogen bonding interactions between the hydroxyl groups of lignin and the anions/cations of ILs are the main driving force to dissolve lignin and cellulose (Ji et al., 2012; Y. Zhang et al., 2017). It is reasonable to expect that this interaction plays a key role in even weakening the recalcitrance of lignin-cellulose structures (Vermaas et al., 2019).

In those studies, the role of chloride anion is considered to be very important as it has a small size to diffuse in solvent and is a potential HBA to lignin, especially around the hydroxyl groups on lignin (Zubeltzu et al., 2020). It was found that in pure solvent, chloride anions, as HBAs, always surround around HBD and choline cation in DES from SDF (Doherty & Acevedo, 2018; Hammond et al., 2016), and the significant impact of the chloride anion–HBD interaction on the solvent properties is also mentioned above. These two types of hydrogen bonding, anion–HBD and anion–lignin/cellulose, may be

closely related and might even be the most important part of interactions between lignin and solvent molecules. Xia et al. (2018) studied the interaction between ChCl/glycerol and lignin and elucidated that the hydrogen bonding interaction between ChCl and glycerol is much weaker than the intramolecular hydrogen bonding in lignin, which indicates that glycerol as HBD is too weak to compete and break down the inner hydrogen bonding network in lignin.

While the role of anion in DES–lignin interaction is straightforward in both MD and DFT studies, the role of choline cation is still controversial. Janesko (2011) reported that *Π*-stacking structure was found between lignin and cation of the IL, which is comparable to the hydrogen bonding interaction between anion and lignin. In some later studies (Ji et al., 2012; Y. Zhang et al., 2017), this π-stacking structure were also observed for lignin, but it seemed weaker than the hydrogen bond with the anion. In a most recent study (Zubeltzu et al., 2020), a π-stacking structure was not found instead, dispersed, non-directional London interactions were identified around either the hydroxyl groups or aromatic rings of lignin. Zubeltzu et al. (2020) explained that the π-stacking structure found in MD is due to the limited dispersion and the lack of charge transfer interaction in MD simulations.

Despite DES having similar properties as ILs, studies about the interaction between lignin and DES are still not clear. Therefore, it is necessary to take a closer look at the interactions between DESs and lignin/cellulose to gain a better knowledge of the mechanism of DESs pretreatment.

CHAPTER 3

A MOLECULAR DYNAMICS SIMULATION STUDY OF CHOLINE CHLORIDE/ETHYLENE GLYCOL

3.1 Introduction

Choline chloride-based DESs are a category of cheap and environmentally friendly solvents that can be used for biomass valorization. Their unique physiochemical properties and tailorability provide flexibility either for biomass fractionation, xylan solubilization, lignin extraction and upgrading. To tune the performance of DESs in biomass pretreatment, it is important to design the solvents with predictable physiochemical properties as well as understand the atom-scaled solvent structure of DES.

While density functional theory (DFT) and *ab initio* molecular dynamics (AIMD) are available for investigations of small molecular interactions, molecular dynamics (MD) simulations are more suitable for calculating the thermodynamic and transport properties of bulk-phase DESs. However, investigations of DESs through MD simulations are still insufficient due to the lack of both computational and experimental supports. Several studies have simulated some common choline chloride-based DESs in order to answer questions, such as the for the low melting points of DESs, the impact of HBD on properties, and hydrogen bonding interactions in DESs. The parameters for DESs such as bond lengths, bond angles and nonbonding interactions were based on force fields intended for biomolecular application, with certain modification. Doherty and Acevedo (2018) developed the OPLS-DES force field to predict the properties of eight ChCl based-DESs and yielded around 1.1% of overall mean absolute errors on density calculations based on MD simulation by GROMACS (Abraham et al., 2015) compared to

experimental values. Gilmore et al. (2018) combined experimental data related to bond structure with simulation through the Empirical Potential Structure Refinement (EPSR) program to illustrate the structural differences between ChCl-urea and ChCl-oxalic acid. Except bond distances and bond angles defined by EPSR, the Lennard-Jones parameters and spatial charges for all atoms were derived from OPLS-AA in their simulation. Perkins et al. (2014) compared the hydrogen bond network for four ChCl based-DESs in order to understand the solvent structures and the role of HBDs in the formation of DESs, and the MD simulation was performed by AMBER with parameters from GAFF (Wang et al., 2004).

All studies mentioned above claimed that the density, as well as other properties in some studies, and showed good agreement with experiments. On the other hand, the solvent structures, which is usually illustrated through the radial distribution function (RDF), are not exactly the same, which might be due to that the partial charge for the same atom type is different among those studies. The difference in the partial charge values can be explained as different charge delocalization in DES. While reproducing properties of DESs is an important step to ensure having good agreement with experiments at the starting point, structural comparison of DESs simulated with different parameters, especially the different partial charge settings, is also necessary to clarify how the charge spreading can affect the liquid structure and to what extent we should believe in the simulation results.

In this work, molecular simulation is used to explore choline chloride/ethylene glycol DES (CCEG) in order to understand their solvent structures. Spatial charge modifications are based on several prior DESs simulation studies, which have achieved

high accuracy for some properties of DESs and are tested by comparing simulated density and diffusion coefficients of DESs to experimental values, as well as the radial distribution function and number of hydrogen bonds formed in the solvent to results from either experiments or computational methods. Microscopic characteristics of those DESs and the partial charges' effects on those characteristics would be established based on the comparison.

3.2 Computational Details

Table 3.1. Partial charges for choline chloride and ethylene glycol [b].

Group name	Set 1	Set 2	Set 3	Set 4
Atom type		Choline Chloride		
N	0.791	−0.15456	0.0452	0.791
C8	−0.1	0.10974	−0.1208	−0.1
H12	0.033	0.05244	0.1074	0.033
C9	−0.131	0.07411	−0.029	−0.131
H13	0.068	0.05244	0.1004	0.068
C10	0.132	0.16201	0.1351	0.132
H14	0.034	0.05244	0.0459	0.034
O9	−0.468	-0.3126	−0.557	−0.468
H15	0.275	0.22008	0.4091	0.275
Cl	−0.8	−1	−0.9	−0.8
Reference	(Doherty & Acevedo, 2018)	(Gilmore et al., 2018)	(Perkins et al., 2014)	(Doherty & Acevedo, 2018)
Atom type[a]		Ethylene glycol		
C1	0.116	0.145	0.1615	0.145
H2	0.048	0.06	0.0328	0.06
O1	−0.56	−0.7	−0.634	−0.7
H1	0.348	0.435	−0.7	0.435
Reference	(Doherty & Acevedo, 2018)	Default charge from OPLSAA	(Perkins et al., 2014)	Default charge from OPLSAA

[a] Atom types for C1, O1, H1 and H2 in OPLSAA (Jorgensen et al., 1996) are 115, 111, 112, 118.
[b] Other parameters and original input files are provided in supporting information.

Materials Studio was used to optimize the geometries of the isolated ions and molecules (BIOVIA, 2011). The optimized potentials for liquid simulations (all atom) (OPLSAA) (Jorgensen et al., 1996) functional form and parameters were used for these

simulations. Partial charges for choline chloride and ethylene glycol were derived from several studies to study their effect on liquid structure in the simulation and better reproduce the thermodynamic properties of DES, and Table 3.1 lists the value and sources of each set. Other parameters for choline chloride were derived from the DES-OPLS force field (Doherty & Acevedo, 2018) and other parameters for ethylene glycol were derived from the OPLSAA force field (Jorgensen et al., 1996). Atom types for choline chloride and ethylene glycol were defined based on their unique positions in the molecular skeletons, as shown in Figure 3.1. Periodic boundary conditions were applied in all directions. Simulation boxes were created with different initial configurations and molecular gap of 3Å using Moltemplate (Jewett et al., 2013). For pure DES systems, 500 choline chloride pairs and 1000 ethylene glycol molecules with a molar ratio of 1:2 are included in the box.

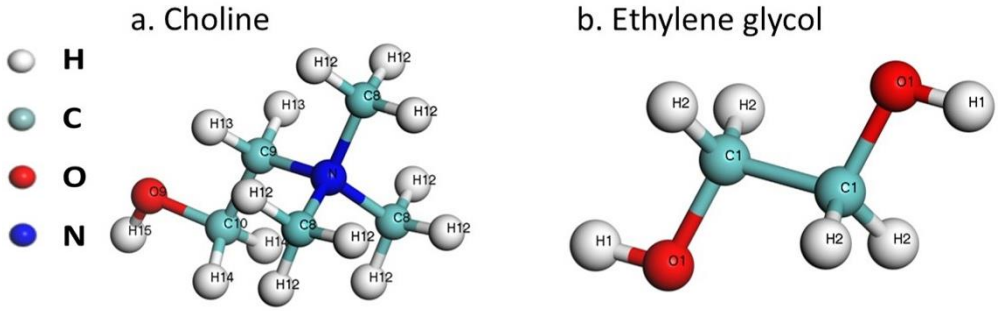

Figure 3.1. Atom types assigned to the (a) choline and (b) ethylene glycol molecules used in MD simulation.

Molecular dynamics (MD) simulations were carried out using the LAMMPS (Plimpton, 1995). Periodic boundary conditions were employed with the global Coulombic cutoff set to 10 Å. Long-range electrostatics were treated with the particle-particle particle-mesh solver (PPPM) with tolerance of 10^{-4}. The 1–2 pairwise interactions (i.e. interactions between two directly bonded atoms) and 1–3 pair

interactions (i.e. interactions between atoms separated by two bonds) are turned off for all specified pairs of atoms by setting weights on 1–2 and 1–3 pairwise Lennard-Jones and Coulombic interactions to 0.0. To apply the same parameters for both intra- and intermolecular interactions (Doherty & Acevedo, 2018), 1–4 intramolecular interactions were scaled by 0.5. The supercell was brought to equilibrium at T = 300 K using Parrinello−Rahman dynamics (fix npt). The pressure was set to 1 atm. Velocities of atoms were randomly assigned with a Gaussian distribution constituent with T = 300 K. The timestep was successively increased to 0.01, 0.1 and 1fs after every 200000 steps to shorten the time to get to the equilibrium state. The output was recorded every 10000 time steps by averaging 10 values sampled every 1000 time steps. From the final coordinates after equilibration, 5 independent production runs with a total time of 10 ns were computed for use in structural characterization and analysis. When the barostat was on, the integration time step was 1 fs. A 2 ns trajectory with 10ps every frame was used for structure and hydrogen bond analysis. The radial distribution function, and number of hydrogen bonds were calculated with VMD (Humphrey et al., 1996). Spatial distribution function was calculated with TRAVIS (Brehm & Kirchner, 2011) and visualized with VMD.

3.3 Results and Discussion

3.3.1 Density and Heat Capacity

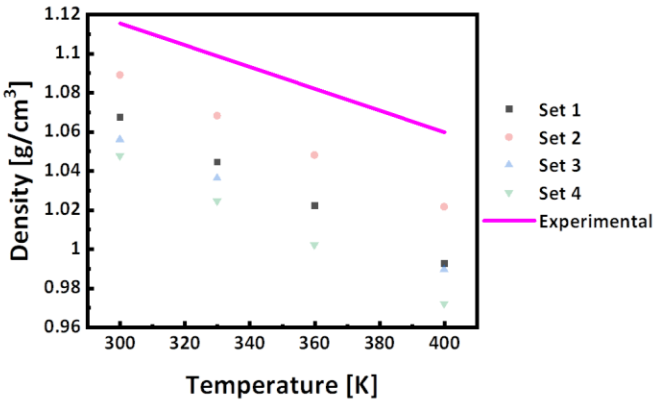

Figure 3.2. Density of CCEG from 300 to 400K for four charge settings. The experimental values are from the study by Harifi-Mood and Buchner (2017).

In Figure 3.2, the simulated densities of 1:2 ChCl/ethylene glycol with four different charge settings are compared with experimental data (Harifi-Mood & Buchner, 2017). All partial charge modifications in this study reproduce density values with error of 3–6%. Set 1 was from OPLS-DES, which was reported by Doherty and Acevedo (2018) and was designed for DES simulations. Anionic charges in Set 1 and Set 4 were scaled by 0.8 from the default values of OPLSAA (Jorgensen et al., 1996), which were intended for better prediction of the properties of DESs by taking the charge delocalization from the anion to the cation into consideration. Although charge delocalization also exists between the anion and ethylene glycol, the amount of charge being transferred to ethylene glycol was relatively small (Zahn et al., 2016). In such cases, charges for ethylene glycol was scaled by 0.8 in Set 1 but remained their given values by OPLSAA in Set 4 to find out whether such a small charge transfer affects the DES properties. Set 3 was from Perkins' study and was scaled by 0.9 from the default values of GAFF (Perkins et al., 2014). Charges in Set 3 are totally different from Set 1 due to the charge assignment methods are

different between OPLSAA and GAFF. The density at 300 K in Perkins' study is around 1.12 g/cm^3, which is closer to the experimental value than the value of Set 3 in Table 3.1. Surprisingly, Set 2, which uses the unscaled charges, gives the closest density value to the experimental value. Shah and Mjalli (2014) also used unscaled charges in their simulations for the same reason. It gave better correlation of density without scaling the charges. In terms of heat capacity, it was found to be almost the same in all settings (around 154 J·mol^{-1}K^{-1}) and underestimated compared to experimental data (190.8–199.2 J·mol^{-1}K^{-1}) (Perkins et al., 2014).

3.3.2 Radial Distribution Function

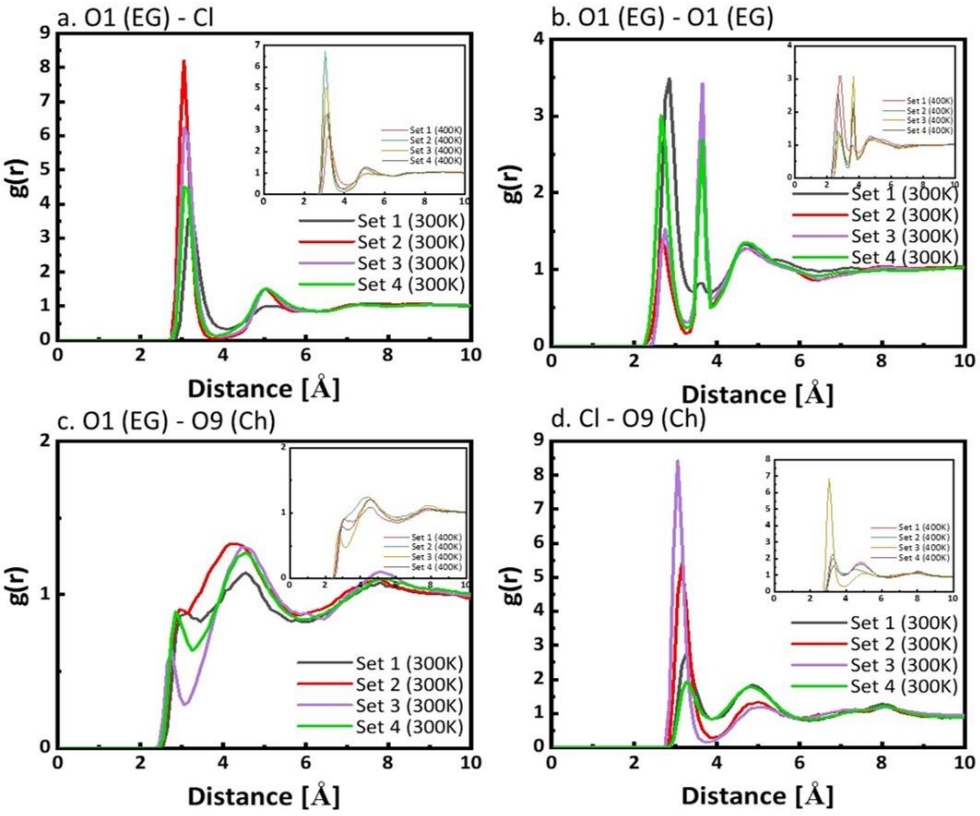

Figure 3.3. Atom–atom radial distribution function of heavy atoms centered at the chloride anion or oxygen atom of ethylene glycol or choline cation.

Besides macroscopic properties (density and heat capacity), the microscopic structure of CCEG with different charge settings is shown in Figure 3.3 at 300 and 400 K. Here, the purpose of the RDF calculation is not to identify the solvent structure but to ascertain how the charge settings could affect the solvent structure of the DES. The distance where the significant peaks appeared for all four pairs of interactions is roughly same, which indicates that no matter what charge settings were used, those pairs would have the strongest interactions at the same distances. For interaction between O1 (EG) and Cl, the heights of the first peak follow the exact same order as the product of charges for O1 and chloride, which is Set 2 > Set 3 > Set 4 > Set 1. It is believed that as the height of the first peak becomes larger, more chloride anions would accumulate around the oxygen atoms of ethylene glycol. Meanwhile, because the two Lennard-Jones parameters (σ and ϵ) in all four settings are the same, the Coulombic forces are the main cause of the peak height differences, which explains why it would follow the order of the product of charges for O1 and chloride.

When it comes to the intramolecular interactions of ethylene glycol and intermolecular interactions with other ethylene glycol molecules, all sets of parameters except Set 1 show two distinct peaks. The second peak likely belongs to the two intramolecular oxygen interactions, as the integration of this peak in coordination number is around 1.00 and the initial distance of the two oxygen atoms is 3.578 Å where is the same position for the appearance of the second peak. Unlike interaction between O1 (EG) and Cl, the peak height in Set 1 has the highest value, followed by Set 4, Set 3, and Set 2, which seemed to have no correlation with the charge on O1. This trend implies that the motion of ethylene glycol might be strongly affected by the interaction with chloride

anion. If ethylene glycol has stronger interactions with chloride anion, then it would have weaker ones with other ethylene glycol molecules.

The interaction of choline cation with ethylene glycol is particularly weak but its interactions with chloride anion are significantly stronger. The product of charges for O9 (Ch) and chloride is 0.5013 for Set 3, which is the highest value among all the settings, indicating that there is a strong Coulombic force between these two atom types. As a consequence, the most distinct structural preference was found between O9 and chloride at the distance of 3.05 Å compared to the same interaction in other sets. However, we do not expect to find that the peak for Set 2 is the second highest one, when the product of charges for O9 and chloride is the lowest. This phenomenon implies that the interaction between O9 and the chloride anion is not only driven by the Coulombic force, but also affected by other factors, such as interactions with the cation or other ethylene glycol molecules. Also, the interaction between O9 and chloride for Set 2 is highly temperature-dependent, which reduces obviously when the temperature was raised from 300 to 400 K. It might be caused by the reduction of hydrogen bonds between O9 and the anion and the increase of velocities of molecules due to the raising of the temperature.

Overall, the most dominant peak is O1 (EG)–Cl for Set 2, Cl–O9 (Ch) for Set 3 and O1 (EG)–O1 (EG) for Set 1 and 4, which reveals the important role of charge settings on the molecular interaction and the further impact on the molecular arrangement as well as the solvent structure. When being compared to another study, peak heights for pairs O1–Cl and O9–Cl for Set 1 are closet to the values in Zahn's study (Zahn et al., 2016), which was obtained from AIMD simulations.

3.3.3 Hydrogen Bond Network

Hydrogen bond networks (Figure 3.4) for these four spatial charges sets also show dramatic differences and the impact of temperature also causes totally different performance with respect to the change of number of H-bonds for each pair. The dominant intermolecular hydrogen bonds are found in O1 (EG)–Cl for Set 2, and O1 (EG)–O1 (EG) for Sets 1, 3 and 4, which has close correspondence with the dominant peak in the RDF (except for Set 3).

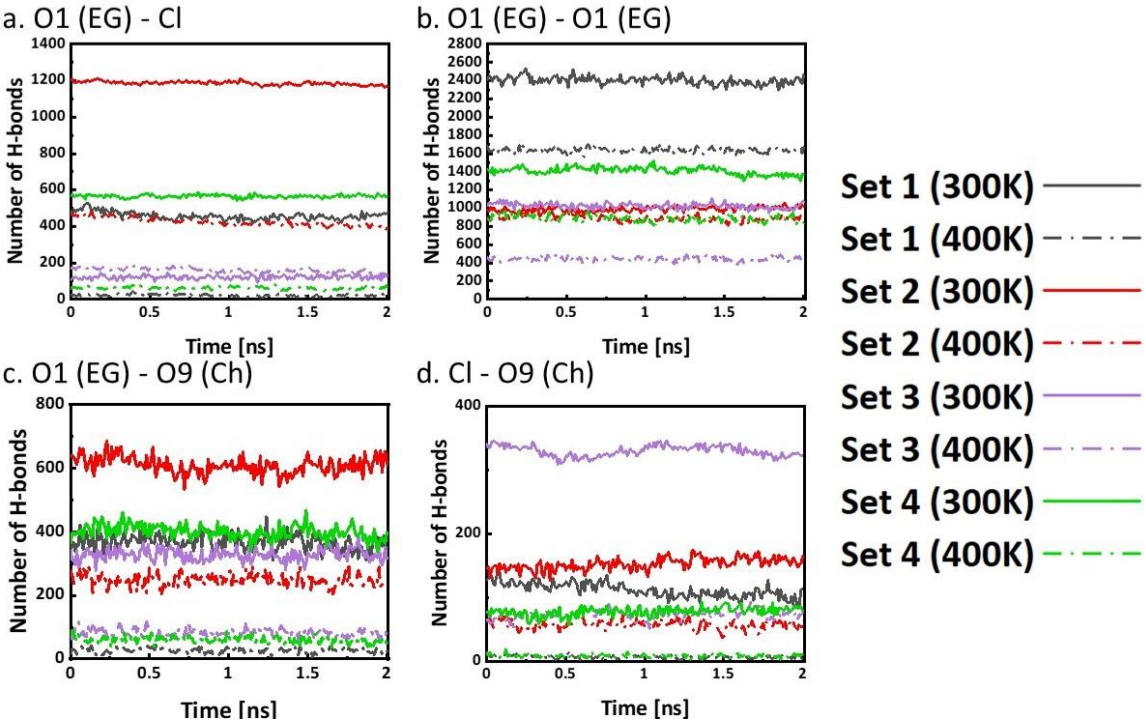

Figure 3.4. Number of H-bonds of CCEG at 300 and 400 K for simulations using different spatial charge sets.

When charge delocalization between ethylene glycol and chloride anion was not considered in the simulation (Set 2), O1 and the anion form the most hydrogen bonds, probably due to the significant contribution of Coulombic forces. The left of O1 in ethylene glycol, which does not couple with the anion via hydrogen bonds, would remain having hydrogen bond interaction with other left O1, and is not affected by increasing the

temperature. When only the charge spreading between O9 and the anion was included (Set 4), the number of O1–Cl hydrogen bonds dropped dramatically to the half of the number in Set 2, following an increase of O1–O1 hydrogen bonds by a few hundred. This further confirms the role of Coulombic forces in the formation of hydrogen bonds, because the difference between the product of charges for O1–O1 and the product of charges for O1–Cl become smaller from Set 2 to 4, which makes the attraction between O1 and other O1 atoms more comparable with the attraction between O1 and the anion. Meanwhile, some atom–atom interactions seemed to be highly temperature dependent, as the O1–O1 hydrogen bonds at Set 4 reduce to roughly the same amount as at Set 2 at 400 K.

Set 1 and Set 3 considered charge spreading for O1, O9, and the anion, but the strength is different. Set 1 assumes more charges transferred among cation, anion, and HBD with a scaling factor of 0.8, while the scaling factor in Set 3 is 0.9. The larger scaling factor indicates more electron density was transferred from O1 and the anion to O9, which causes O9 in Set 3 to be more negative than O9 in Set 1. Interestingly, in Set 3, O9–Cl hydrogen bonds are significantly more common, reaching to more than twice the amount using Set 1. Meanwhile, O1–Cl hydrogen bonds only left less than half of the amount of Set 1. This can be explained by the stronger interaction between O9 and the anion largely driven by Coulombic forces in Set 3, which probably constrained the diffusion of the anion at the beginning, limiting the following interaction between O1 and the anion. With less O1 hydrogen bonding with Cl, inter- and intra- molecular interactions of ethylene glycol molecules in Set 1 become more common compared to other three sets, leading to the increase of O1–O1 hydrogen bonds. Compared to Set 4

which includes charge spreading of O1, would greatly determine how ethylene glycol molecules interact with each other.

3.3.4 Spatial Distribution Function

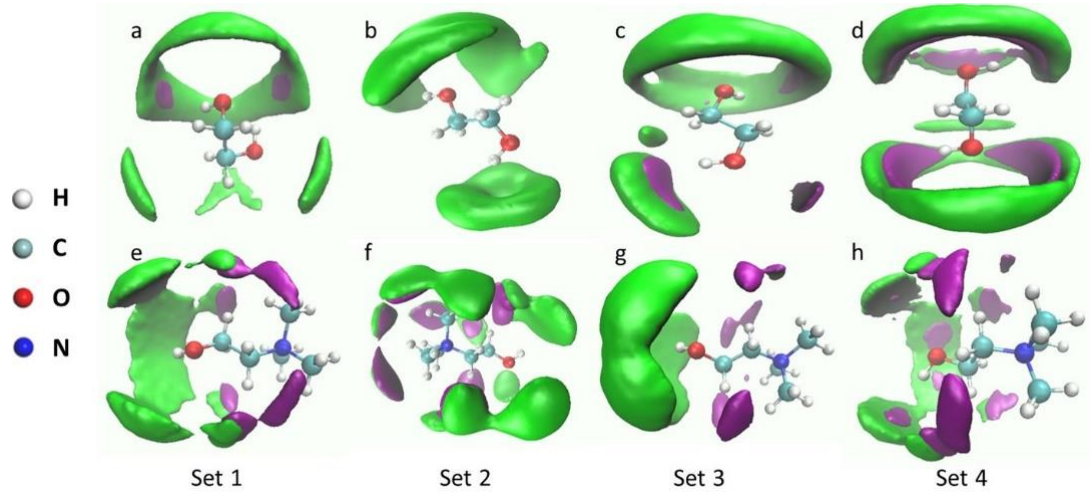

Figure 3.5. Spatial distribution function of chloride anion (green) and oxygen atom of ethylene glycol (purple) centered around ethylene glycol (top) and choline cation (bottom). Isovalue for all chloride anion is 3g/cm^3 and isovalue for all oxygen atom is 1.6g/cm^3. O1, O4, O8 in purple, and O7, O6 in cyan.

The spatial distribution function (SDF) (Figure 3.5) visualizes the atomic arrangement around the HBD and the choline cation. In Set 2, chloride ion seems to be closer to and largely covers the oxygen atoms of ethylene glycol, leaving other O1s little space to contact it (i.e., the purple block for O1 is hidden inside the green block for Cl in Figure 3.5), which corresponds to the most hydrogen bonds between O1 and the anion found in Figure 3.4. In Set 4, O1 is drawn near other O1 atoms, which is in contrast to Set 2, and gave less opportunity for the anions to connect with O1 via hydrogen bonds. As mentioned in section 3.3.1, the greatest difference between Set 4 and any one of the other sets is that partial charges for ethylene glycol were not scaled while charges for choline chloride were. This inconsistent scaling strategy caused the improvement in interaction strength for O1–O1, and also reduced the uneven distribution for chloride around the cis-

and trans- oxygen atoms. On the other hand, when the scaling strategy is inconsistently applied to both ethylene glycol and choline chloride and the scaling factor is reduced from 1 (Set 2) to 0.9 (Set 3) to 0.8 (Set 1), not only the partial arrangement of the anion around O1 shows high dependance on the *cis*- and *trans*-position of oxygen atom, but also becomes more dispersive. When it comes to the molecules' positions around the cation, a significant difference was found. When partial charges were not scaled (Set 2), which assumes that no charge delocalization was included in DES, the anions also accumulate around the nitrogen atom of the cation. Once the impact of the charge delocalization on the formation and solvent structure of DES was included in the simulations via scaling partial charges of all solvent atoms, the amount of the anions accumulating around the nitrogen atom decreases significantly (Figure 3.5 e–h). However, it is not clear whether such accumulation around the nitrogen atom for the anions is correlated with the charge delocalization. Other factors, such as the spatial charge of the nitrogen atom, might also contribute to this phenomenon.

3.4 Conclusions

This study selected several partial charge sets from recent simulation studies of DES, aiming to understand how the partial charges would affect the reproduction of the thermodynamic properties of DESs as well as the formation of DESs. Density here was found to be insufficient to decide whether the force field can reproduce the actual solvent characteristics. On the other hand, the partial charge sets were found to play important roles in the dynamic molecular arrangement of DESs. Although the distance between atoms remained the same in all the charge sets, the strength of interactions for those atoms varied a lot. In classical MD with nonpolarized force field which does not include

the charge delocalization in the solvents, a scaling factor is applied on the default partial charges provided by selected force field to mimic the charge spreading phenomenon, which is considered to be the reason for the unique physical features of DESs (such as low melting point) so that the simulated physiochemical properties can get closer to experimental data. Based on the results shown here, charge spreading might also be the key to the unique molecular arrangement of DES, which can be very different depending on whether the scaling factor is applied or not. However, the accuracy of the density would not necessarily indicate such information, which would mislead one into thinking a model is more accurate than it is. Except the recommendation of choosing a polarized force field which charge delocalization is also considered in classical MD mentioned in many recent studies, the current feasible way to ensure the reliability of DES simulation is carefully investigating the charge setting. In the meantime, comparing more types of experimental parameters with simulated data, especially those parameters which can reveal the liquid structures, is necessary to achieve better simulation.

CHAPTER 4

UNDERSTANDING LIGNIN DISSOLUTION BEHAVIOR IN DEEP EUTECTIC SOLVENTS: A MOLECULAR DYNAMICS STUDY

4.1 Introduction

Deep eutectic solvents (DESs), a cheap and environmentally-benign analog of ionic liquids (ILs), can serve as effective solvents for biomass fractionation and lignin dissolution (Lynam et al., 2017). DESs can be endowed with various physicochemical properties by combining different constituents. However, it remains a challenge to predict DES performance on lignin extraction efficiency due to heterogenous nature of lignin. Many experimental efforts have been made to develop versatile DESs for lignin extraction. Due to the lack of understanding of the role of DESs and their constituents in lignin dissolution, the selection of DESs for biomass fractionation largely relies on trial and error. Therefore, there is a critical need for advancing the understanding of DES–lignin interactions to facilitate the rational design of DESs for biomass fractionation and lignin extraction.

Computational chemistry has been used to elucidate DES–lignin interactions both qualitatively and quantitively. In a recent study, density functional theory (DFT) revealed hydrogen bonding interactions between ChCl/glycerol DES and lignin are too weak to compete with hydrogen bond network in lignin, resulting in insignificant dissolution of lignin from woody biomass. On the other hand, the addition of a Lewis acid (e.g., $AlCl_3$) drastically increased the ability of ChCl/glycerol to dissolve lignin via the formation of supramolecular complexes between the acid and DES. The complexes allow the multisite bridging ligands with acidic sites to cleave both the H-bonds and ether bonds in the

lignocellulose complex. In another study, Ji and Lv (2020) investigated the interaction between ChCl/lactic acid and veratrylglycerol-β-guaiacyl ether (VG), a lignin dimer, via both DFT and MD simulations. They revealed that the main noncovalent interactions were caused by the π-stacking configuration between the C-H bonds of DES and the aromatic rings of VG as well as the hydrogen bonding between the hydroxyl groups of both the DES and VG. Their finding of a sharp peak at a distance of 2 Å in the RDF between lactic acid and hydroxyl groups of VG suggests that compared to chloride anion lactic acid forms more hydrogen bonds with lignin.

Hydrogen bonding interaction is the main intermolecular interaction between lignin and DES. Meanwhile, it could also interrupt the strong association between lignin and cellulose which contributes to the recalcitrance of biomass. The strong association between lignin and cellulose means that lignin always tends to adhere to the surface of cellulose. This phenomenon was found to be surface-dependent via MD simulation (Besombes & Mazeau, 2005a). On the hydrophilic surface of cellulose lignin would connect with cellulose closely via hydrogen bonds, while on the hydrophobic surface the aromatic rings of lignin would be restricted on the surface and stay parallel. One explanation for lignin adsorption behavior on the hydrophobic surface is that lignin with hydrophobic nature tend to repulse water and adhere to the hydrophobic surface. This implies that surface adsorption can be induced and governed by a solvent environment.

As one main purpose of biomass fractionation is to separate lignin from lignocellulosic complex (Thakur et al., 2014), we hypothesize that an effective DES should form strong hydrogen bonds with lignin to compete with the intermolecular hydrogen bonding interactions in lignin as well as intramolecular ones between lignin and

cellulose. To test the hypothesis, DESs composed of choline chloride as a hydrogen-bond acceptor (HBA) and ethylene glycol, lactic acid, or formic acid as a hydrogen-bond donor (HBD) were used to study lignin dissolution behavior via MD simulation. These DESs have been shown to perform differently in biomass pretreatment(Al Ameri, 2017; Chen et al., 2018a; Z. Chen et al., 2019). Two classical lignin models (i.e., guaiacylglycerol-β-guaiacyl ether (GG), Adler's lignin) were used to identify the structural changes of lignin in the solvents. Furthermore, lignin–cellulose interactions were also simulated for solvent-driven preferential association of lignin with cellulose in a DES system.

4.2 Computational Details

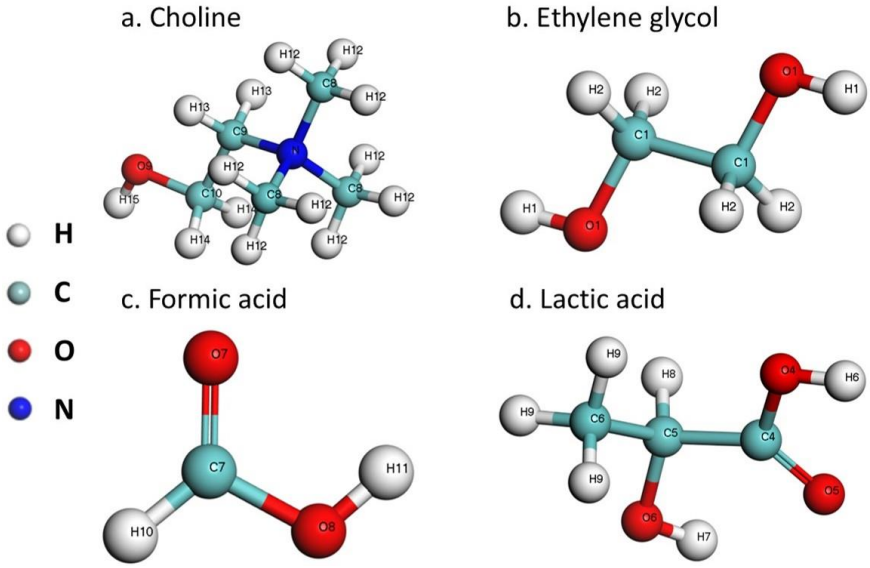

Figure 4.1. Atom types assigned to the choline and HBD molecules used in MD simulation.

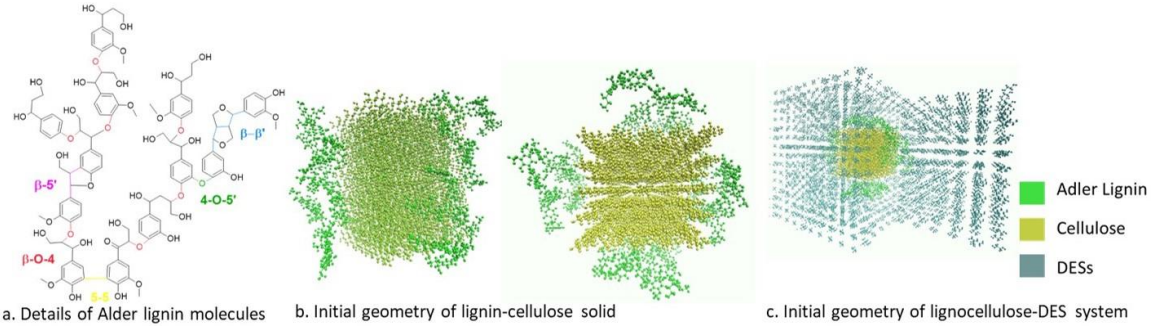

Figure 4.2. Initial geometries of lignin and cellulose crystalline

We modeled three choline chloride-based DESs with ethylene glycol, formic acid, and lactic acid as an HBD (hereafter referred to CCEG, CCFA, and CCLA, respectively). The molar ratio of a HBA to HBD was 2:1. Atom assignments for all the compounds were defined based on their unique positions in the molecular skeletons, as shown in Figure 4.1. For lignin, two model compounds were used: guaiacylglycerol-β-guaiacyl ether (hereafter referred to GG lignin), a commonly used lignin dimer (Jia et al., 2011; Y. Zhang et al., 2017; Zhang et al., 2019), and Adler lignin (Figure 4.2a), a softwood lignin model compound including all the common linkages in lignin (Rismiller et al., 2018; T. Zhang et al., 2017; Zhang et al., 2016). The purpose of using two lignin models was to investigate the effects of lignin molecular weight on its structural changes when being dissolved by a DES. An Adler lignin molecule contains 12 lignin monomers (G unit) covalently bonding via seven β-O-4 linkages, one β-5, one 5-5′ linkage, one 5-O-4 linkage, and one β-β linkage (Figure 4.2a). To study the DES effects on lignin extraction from biomass, especially disassociation of lignin from cellulose, a crystalline cellulose–lignin block was modeled to mimic lignin's adsorption on the cellulose surface. Our model crystalline cellulose was composed of 41 chains with a chain length of 10 monomers (i.e., glucose). The crystalline cellulose–lignin block consists of one

crystalline cellulose surrounded by 8 Adler lignin models. Two lignin molecules are on each (200) face and (010) face (Figure 4.2b), and the cellulose–lignin bulk was placed at the center of the supercell (Figure 4.2c). Geometries for all DES molecules were optimized via VASP calculations in Materials Studio (BIOVIA, 2011). The partial charges for choline cation in CCFA and in CCLA, formic acid, lactic acid, and GG lignin are the Mulliken atomic charges derived from the output file of the VASP calculations. Partial charges of choline cation in CCEG is from the work reported by Gilmore et al. (2018) and partial charges of ethylene glycol are from the OPLSAA force field.(Jorgensen et al., 1996) To decide the fair values for partial charges of DES molecules, we used partial charges from relevant studies or VASP calculations in several independent simulations for each DES (not shown). The charges resulting in better density reproduction of the experimental data would be picked for the following simulations. Partial charges and the geometry of Adler lignin and cellulose were from a prior study by Rismiller et al. (2018). Force field parameters except partial charges for choline chloride were derived from the DES-OPLS force field (Doherty & Acevedo, 2018) and the parameters for HBDs, lignin models, and cellulose were derived from OPLSAA force field (Jorgensen et al., 1996).

Four MD simulation systems were built for each DES: DES, DES–GG lignin, DES–Adler lignin, and DES–lignin–cellulose. Molecules were randomly arranged by being assigned with a large molecular gap (3 Å) via Moltemplate (Jewett et al., 2013). For the DES systems, 500 ChCl pairs and 1000 HBDs were included in the box. For the DES–GG lignin systems, 500 choline chloride pairs, 1000 HBD molecules, and 120 lignin

dimers were included in the box. The total molecular weight of lignin in the box was 38440.8 g/mol with 2040 carbon atoms and GG lignin concentration in a DES solvent was around 19-25 wt%. For the Adler lignin–DES systems, 500 choline chloride pairs, 1000 HBD molecules, and 18 Adler lignin molecules were included in the box. The total molecular weight of lignin in the box was 39528 g/mol with 2080 carbon atoms and Alder lignin concentration was around 13-17 wt%. Lignin concentration in the solvent systems are similar to that in experimental studies on lignin dissolution by DES.(Q. Liu et al., 2019) For DES–lignin–cellulose systems, 500 choline chloride pairs, 1000 HBD molecules, 8 Adler lignin molecules, and one crystalline cellulose were included in the supercell.

Molecular dynamics (MD) simulations were carried out using the LAMMPS (Plimpton, 1995). Periodic boundary conditions were employed in all Cartesian directions. Long-range electrostatics were treated with a particle-particle particle-mesh solver (PPPM) with tolerance of 10−5 and cutoff of 10 Å. The 1–2 pairwise interactions (i.e. interactions between two directly bonded atoms) and 1–3 pair interactions (i.e. interactions between atoms separated by two bonds) are turned off for all specified pairs of atoms by setting weights on 1–2 and 1–3 pairwise Lennard-Jones and Coulombic interactions to 0.0. To apply the same parameters for both intra- and intermolecular interactions (Doherty & Acevedo, 2018), 1–4 intramolecular interactions were scaled by 0.5. The supercell was brought to equilibrium at T = 300 K using Parrinello−Rahman dynamics (fix npt). The pressure was set to 1 atm. Velocities of atoms were randomly assigned with a Gaussian distribution constituent with T = 300 K. The timestep was successively increased to 0.01, 0.1, and 1fs after every 200000 steps to shorten the time

to get to the equilibrium state. After that, the timestep would be 1 fs for the rest of the simulations. Besides the above relaxation process, different strategies were supplemented before or after the process. For Adler lignin–DES systems, energy minimization was first performed to the supercell before the relaxation process with tolerance of 10−4 for energy and of 10−6 for force. For lignin–cellulose–DES systems, initial temperature was set to 400 K during the relaxation process and for another 10 ns to accelerate the diffusion of solvent molecules. Temperature was then decreased to 300 K for at least 20 ns before analysis. The output was recorded every 10000 timesteps by averaging 10 values sampled every 1000 timesteps. From the final coordinates after equilibration, 5 independent production runs with a total time of 10 ns were computed for use in structural characterization and analysis. A 2 ns trajectory with 10 ps every frame was used for further analysis. To clarify the molecular arrangement in the systems, the radial distribution function, and number of hydrogen bonds (H-bonds) were calculated with VMD (Humphrey et al., 1996). The H-bonds are defined as the distance between the donor (D) and acceptor (A) less than 3.5 Å and the angle D-H-A less than 150°. Coordination numbers (CN) is the integration of the first peak of each radial distribution function. Spatial distribution function was calculated with TRAVIS (Brehm & Kirchner, 2011) and visualized with VMD. To characterize the lignin structures, the solvent-accessible surface area (SASA) and the radius of gyration (Rg) were computed by VMD (using the command “measure sasa” and “measure rgyr”). The radius of the probe is 1.4 Å in the calculation of SASA. To quantify the degree of association between lignin and cellulose, number of close contact between cellulose and lignin (either for all

atoms in lignin or for the center of mass of the aromatic rings in lignin) is calculated and the close contact is defined as that distance between two atoms should be less than 3.5 Å.

4.3 Results and Discussion

4.3.1 Force Field Validation

Table 4.1. Density of DESs simulated in this study at 300 K.

	Simulated	Experimental	Error (%)	Reference
CCEG	1.089046	1.11704 (at 298 K)	−2.506	(Leron et al., 2012)
CCFA	1.109413	1.16 (at 297 K)	−4.361	(Lynam et al., 2017)
CCLA	1.129468	1.178 (at 300 K)	−4.12	(Francisco et al., 2013)

Table 4.1 lists the density of three DESs simulated in this study. It shows good agreements with several experimental studies (Francisco et al., 2013; Leron et al., 2012; Lynam et al., 2017). Errors range from −2.5% to −4.4% likely due to the slightly underestimated density for simulation.

4.3.2 Solvent Structure

4.3.2.1 ChCl/Ethylene Glycol

Table 4.2. Comparison of Radial Distribution Function Maximum Peak Heights, *g(r)*, for the First Solvation Shell and Their Distances (R_{max} in Å) for ChCl/ethylene glycol.

	(Zahn et al., 2016)[a]	(Doherty & Acevedo, 2018)[a]	This work		(Perkins et al., 2014)[b]	This work
Pair	$R_{max}(g(r))$			Pair	$R_{max}(g(r))$	
Cl–N	4.2(3.5)	4.28(4.6)	4.55(3.54)	Cl–H15	2.2(11.8)	2.25(4.53)
Cl–O9	3.05(3.9)	3.08(2.5)	3.35(2.29)	Cl–H1	2.3(8.8)	2.05(15.30)
Cl–O1	3.10(4.0)	3.06(4.6)	3.05(8.20)	Cl–H2	3.5(1.7)	3.45(1.835)

[a]: Zahn's and Doherty's simulation were both conducted at 375 K.
[b]: In Perkins' work, temperature for RDF calculation is nonspecific, probably around 298 to 330 K.

The solvent structure of ChCl/ethylene glycol (CCEG) has been studied by Zahn et al. (2016) using AIMD, Doherty and Acevedo (2018) using classical MD as well as by Perkins et al. (2014) using classical MD. Except the maximum peak height of pair Cl–O1,

this simulation of CCEG was able to reproduce peak shapes and positions from the AIMD RDF (Zahn et al., 2016) and MD simulation RDF using OPLS-DES force field (Doherty & Acevedo, 2018) (shown in Table 4.2). By integrating the RDF of pair Cl-N within the distance up to 475 pm, 1.27 anions reside on average around the cation, which is close to the value (1.22) reported from the AIMD simulation and integrated within distance up to 450 pm. The interaction between chloride anion and the hydroxyl groups of ethylene glycol is stronger with a peak height of 15.30 than the interaction between the anion and the hydroxyl group of choline cation in this study. One of the reasons can be the different value of charges assigned to H15 of ethylene glycol and to chloride anion. In this work, the charge of H15 is 0.435, which is more attractive to chloride anion with charge of −0.1, while in Perkins' work (Perkins et al., 2014), the charge of H15 and chloride anion are −0.7 and −0.9, respectively. Similarly, the difference between charge of H15/O9 and charge of H1/O1 in simulation by Doherty et al. (Doherty & Acevedo, 2018) is smaller than the difference of charges of these two types of hydrogen/oxygen atoms in this study, which leads to less difference on the peak height between pair Cl–O9 and pair Cl–O1.

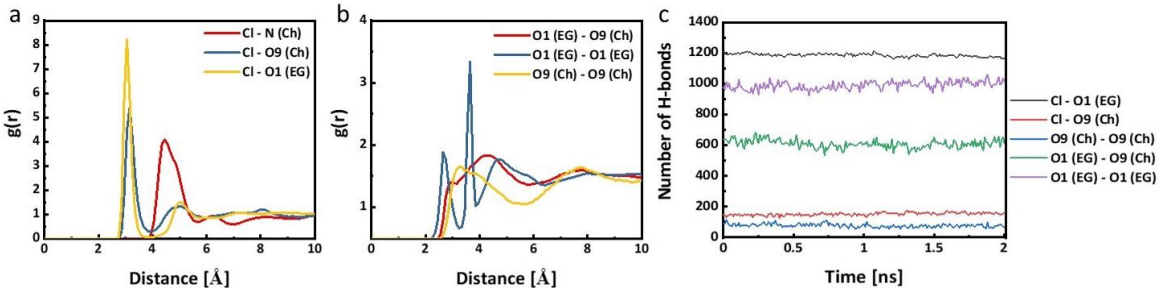

Figure 4.3. Atom-atom radial distribution function of oxygen atoms centered around (a) chloride anion, (b) oxygen atom of ethylene glycol or choline cation, (c) number of hydrogen bonds per frame for CCEG.

In Figure 4.3a&b, the atom–atom RDF illustrates the close contacts in CCEG system.

Chloride anion involves the first two of the close contacts in this system: one of them is between chloride anion and the hydroxyl groups of ethylene glycol, and the other is between chloride anion and the hydroxyl groups of choline cation. For the hydroxyl group of choline cation, besides the dominant interaction with chloride anion, no preference was found when interacting with either ethylene glycol or choline cation as it is shown in Figure 4.3b. Due to such strong interaction with chloride anion, hydroxyl groups between ethylene glycol molecules interact relatively weakly with each other with the first peak height of 1.387. The second sharp peak in orange (at 3.65 Å) for Figure 4.3b is most likely due to the intramolecular interaction of ethylene glycol with the coordination number of 1.162.

In Figure 4.3c, hydrogen bonds network in CCEG was presented with number and types of hydrogen bonds over the sampling time of 2 ns. Because there are two hydroxyl groups in each ethylene glycol molecule, it is more likely for ethylene glycol to form hydrogen bonds with other molecules playing the role of either a HBD or a HBA. Chloride anion forms the most hydrogen bonds with ethylene glycol molecules due to its small size, following ethylene glycol and choline cation, which agrees with the RDF results.

4.3.2.2 ChCl/Formic Acid

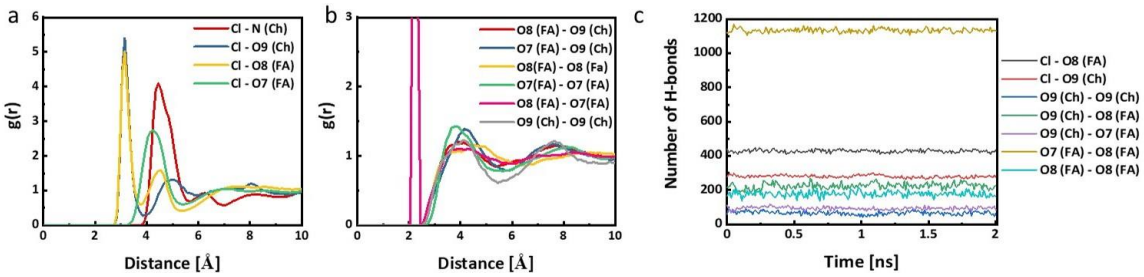

Figure 4.4. Atom–atom radial distribution function of heavy atoms centered around (a) chloride anion, (b) oxygen atom of formic acid or choline cation. (c) number of hydrogen bonds per frame for CCFA.

Figure 4.4a&b shows the solvent structure of ChCl–formic acid (CCFA) including RDF and hydrogen bonding network of this solvent, which to our knowledge has not been reported before. Similar to CCEG, chloride anion also has the first two strongest interactions with both hydroxyl groups of choline cation and formic acid, but the latter one is not as strong as with ethylene glycol. Although formic acid also has two oxygen atoms as ethylene glycol does, one of the oxygen atoms is carboxyl oxygen and is not able to form hydrogen bonds with chloride anion, which makes formic acid less competitive as a HBD. In Figure 4.4b, the interactions among oxygen atoms from choline cation and formic acid reveal that no distinct structural preference exists between choline cation and formic acid or within either the cation or the HBD. The significant intensity peak between O8 and O7 of formic acid should be mainly caused by intra-molecular interaction, which can be further validated by coordinates number of 1.00. Unlike CCEG, the dominant type of hydrogen bonds is pair O8–O7, and it is 160% more than hydrogen bonds of pair Cl–O8 as shown in Figure 4.4c. Besides intra-molecular interaction, inter-molecular interaction might also exist and lead to the formation of single dimer unit, which is common in monocarboxylic acid (D'Agostino et al., 2011). The following two

dominate pairs which connect via hydrogen bonds are between chloride anion and O8 of formic acid as well as O9 of choline cation, which is roughly half of the corresponding pairs (Cl–O1 and Cl–O9) in CCEG. Since in CCFA, only one oxygen atom (O8) of formic acid can act as HBD, chloride anion needs to compete with O7 of formic acid. Clearly, O7 of formic acid takes more advantages in this competition which credits to the intramolecular close contact. The reduction of hydrogen bonds between chloride and formic acid leads to more chloride anion forming hydrogen bonds with choline cation, and thus less cation interacts with formic acid.

4.3.2.3 ChCl/Lactic Acid

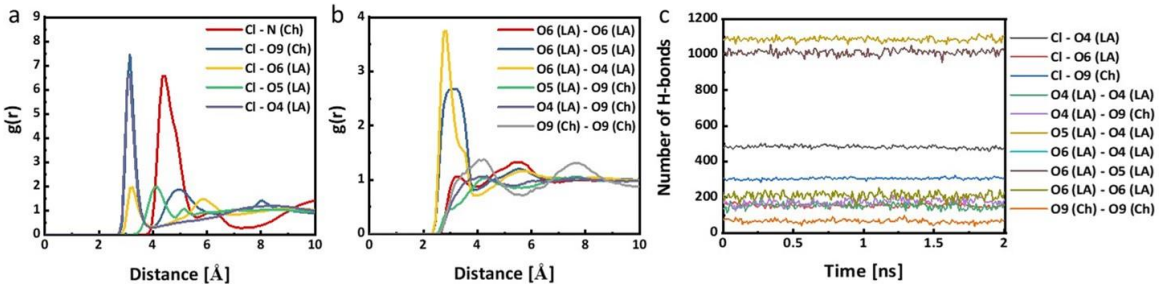

Figure 4.5. Atom–atom radial distribution function of heavy atoms centered around (a) chloride anion, (b) oxygen atom of lactic acid or choline cation, (c) number of hydrogen bonds per frame for CCLA.

Lactic acid, on the other hand, has one carboxyl group and one hydroxyl group with total three oxygen atoms. As expected, chloride anion has close contacts with both O6 from carboxyl group and O4 from hydroxyl group as well as with hydroxyl groups of choline cation. However, interaction with chloride anion and O6 is far less strong as interaction between chloride anion and O1, which is possibly due to the steric hindrance of the carbon chain of lactic acid. In Figure 4.5b, peaks for pair O6–O4 and O6–O5 had a small shoulder and bimodal distribution, respectively due to the existence of both the intra- and intermolecular interaction of lactic acid. In Figure 4.5c, the first three pairs that

have the most hydrogen bonds (O6–O4, O4–O5, O6–O5) in ChCl/lactic acid (CCLA) all belong to the inter- and intra-interaction of three oxygen atoms (O4, O5, O6) of lactic acid. This indicates that akin to formic acid, the self-aggregation of lactic acid also happens in this solvent, and not only a dimer, a trimer and a tetramer might appears, which was found in water and methanol via some spectroscopic techniques (Losada et al., 2008). Although the self-aggregation becomes even stronger for lactic acid, lactic acid still has more intensive interaction with choline chloride compared to formic acid because lactic acid has three oxygen atoms available for any types of hydrogen bond interactions.

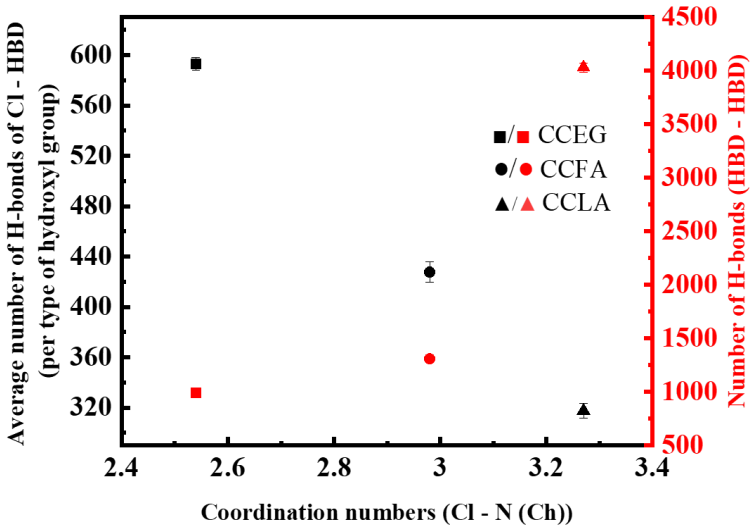

Figure 4.6. Number of H-bonds of Cl–HBD (blue) and HBD–HBD (red).

When three types of DESs being compared, one interesting trend can be found. As self-aggregation of HBD become more common (Figure 4.6), hydrogen bonds formed between chloride anion and the hydroxyl groups of HBD become less. Meanwhile, more chloride anion tends to accumulate around the hydroxyl group and nitrogen atom of choline cation, which causes the increase of both H-bonds of pair Cl–Ch and coordination numbers between chloride and nitrogen. Coordination number of pair Cl–O9 in CCFA

and CCLA is roughly the same while coordination number of pair Cl–N in CCLA (3.27) is larger than CN in CCFA (2.98) and CN in CCEG (2.54). Interaction between chloride anion and nitrogen atom is electrostatic and therefore is non-hydrogen bonded contact.

Spatial distribution functions (SDFs) can provide more insights with respect to the preferential positioning of chloride anion and oxygen atoms of HBD surrounding both the cation and HBD of the solvents. Green, purple, and cyan blocks in Figure 4.7 represent the most probable sites of finding chloride anion and oxygen atoms of HBD, respectively. As expected, more chloride anions in SDFs around choline cation accumulates from CCEG to CCFA to CCLA. One of the reasons can be that the self-aggregation of HBD can limit the mobility of the whole system which also slows down the anion to get close with HBD. Similar conclusion was also reported for maline (choline chloride–malonic acid DES) in the study by D'Agostino et al. (2011). The other explanation is that the electrostatic force from nitrogen atom becomes comparable to hydrogen bonding interaction as the intensity of the latter one between chloride anion and HBD gets weaker from CCEG to CCFA to CCLA. Meanwhile, the HBDs are also attracted by nitrogen atom in a similar manner.

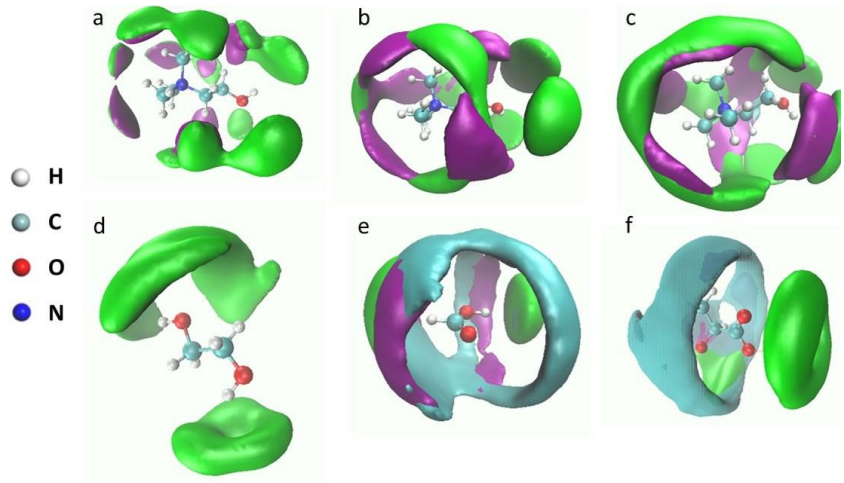

Figure 4.7. Spatial distribution function of chloride anion (green) and oxygen atom of HBD centered around choline cation (top) and HBD (bottom). CCEG (a, d), CCFA (b, e), CCLA (c, f). Isovalue for all chloride anion is 3g/cm^3 and isovalue for all oxygen atom is 1.6g/cm^3. O1, O4, O8 in purple, O7, O6 in cyan.

Self-aggregation of HBD was barely found in CCEG. Instead, ethylene glycol tends to form a complex structure with chloride anion near its hydroxyl groups. Chloride anion was also found near the hydroxyl groups of two carboxylic acids connecting via hydrogen bonds, and some of the anions interact with carbon atom of formic acid electrostatically. However, carboxylic acids have more intensive interaction with other carboxylic acids in CCFA and CCLA. O7s of formic acid (cyan in Figure 4.7b&e) surround O8 from most directions leading to a higher probability of forming hydrogen bonds with O8, while chloride only gathers near the two hydrogen atoms. Assembles around carbon atom of formic acid is likely due to electrostatic interaction, analogous to interaction between chloride and nitrogen. O6 of lactic acid (cyan in Figure 4.7c&f) is accumulated as a circle around O6, however, the dominant atom around O4 is chloride anion. This implies that the self-aggregation of lactic acid mostly happens on the middle of the molecule, where O6 is the main HBD.

In short, polyol-DES and carboxylic acid-DES have different ordered solvent

structure highly depending on the hydrogen bonding interactions of the functional groups. The HBDs have different preference on hydrogen bonding interaction with chloride anion and other oxygen atoms of HBDs. In CCEG, chloride anions and the oxygen atoms from other ethylene glycol molecules are both good HBAs. Chloride anions have smaller size and thus more flexible when hydrogen bonding with ethylene glycol molecules. In contrast, carboxylic acid takes more advantages on forming hydrogen bonds with other carboxylic acids especially when the acid has more than two oxygen atoms, and they have more types of bonded pairs if HBD has more than two functional groups. In such cases, carboxylic acid dimer would appear and reduce the flexibility of choline chloride, which causes less hydrogen bonds between chloride anion and HBDs.

4.3.3 Structural changes of GG and Adler lignin in DES

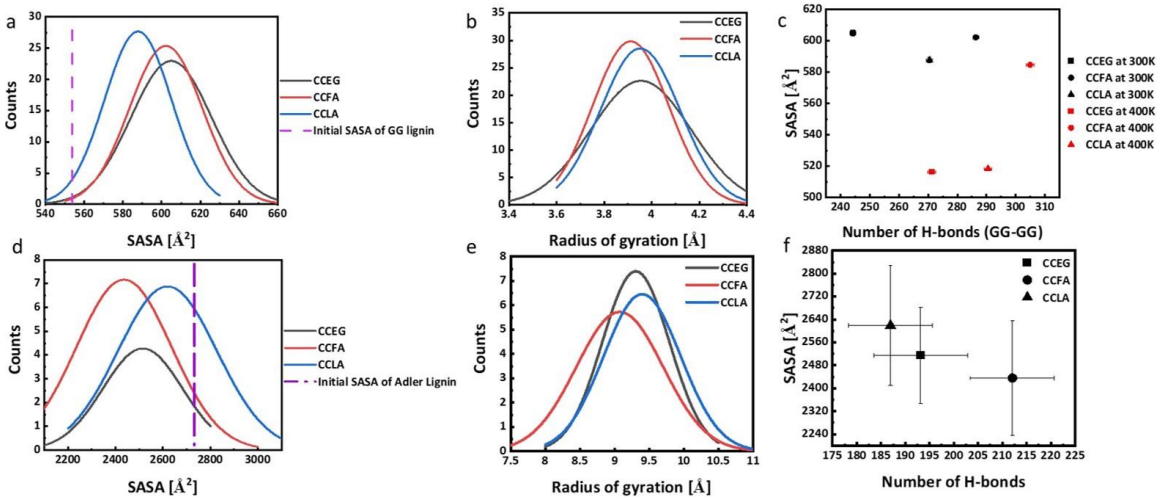

Figure 4.8 Average solvent-accessible surface area (SASA) distribution, radius of gyration (R_g) distribution for lignin, and correlation between number of H-bonds for lignin-lignin and average SASA in different DESs for GG (a, b, c) and Adler lignin (d, e, f).

Calculations of the average solvent accessible area (SASA) and the radius of gyration (R_g) are presented in Figure 4.8 to characterize both lignin models' structural changes in the three DESs. Larger values of SASA and R_g indicates a more open and extended structure for lignin. The R_g and SASA of either lignin model in the three DESs are statistically similar because the lignin model's aggregation and extension are minimal. However, GG lignin and Adler lignin showed different structural changes. For GG lignin, SASA in CCLA (587.8 Å^2) is slightly smaller than in CCFA (602.2 Å^2) and CCEG (604.97 Å^2). It implies that GG lignin in CCEG and CCFA are more openly interacting with the solvent at 300 K. For Adler lignin, it is observed that the average SASA in each DES system follows the order CCLA–AL (2618.992 Å^2) > CCEG–AL (2514.805 Å^2) > CCFA–AL (2435.845 Å^2), which is opposite to the structural responses of GG lignin. Overall, most GG lignin molecules in DESs have larger SASA values that that from the

initial geometry, while Adler lignin followed an opposite trend, with the majority having a less open structure compared to that from the initial geometry. Figures 4.8c&f illustrate how the SASA and lignin–lignin H-bonds change. For GG lignin, we included simulations under two temperatures (i.e., 300, 400 K). The SASA of GG lignin and lignin – lignin H-bonds changed dramatically in CCEG and CCLA when the temperature changed. Meanwhile, HBD–HBD and HBD–anion H-bonds also reduced at 400K (not shown), which shows that for most intermolecular interactions the strength of the hydrogen bond interactions is temperature-dependent. In contrast, the average SASA of Adler lignin shows a negative correlation with lignin–lignin H-bonds (Figure 4.8f). Such a correlation was not observed with GG lignin at either temperature. In general, a lignin molecule with a more extended structure should have a larger SASA and less intramolecular H-bonds.(Smith et al., 2016) The negative correlation in Adler lignin exemplifies this phenomenon, indicating that the intramolecular H-bonds contribute to a large part of lignin–lignin H-bonds of Adler lignin. In contrast, for GG lignin, intermolecular H-bonds more likely make up a large part of lignin–lignin H-bond, especially at 300 K. Upon the interactions with DES molecules and other lignin molecules, the SASA of GG lignin becomes larger than that in the initial geometry at 300 K, causing less intramolecular interaction of the lignin. When the temperature rises to 400 K, the SASA of GG lignin decreases, and the lignin–lignin H-bonds increase. The decrease of SASA indicates that the lignin molecules become more self-aggregated, while the increase of lignin–lignin H-bonds should be mainly contributed by the intramolecular H-bonds of lignin molecules. Another interesting difference between the two lignin models is that Adler lignin has a broader distribution of SASA in DESs than

GG lignin, which implies that its structural change is more sensitive to solvent interactions.

4.3.4 Interaction between chloride anion and lignin

Oxygen atoms in lignin are categorized in two ways in this work. In the first way, oxygen atoms are divided into three types, OA, OP, and OS. OA represents the two oxygen atoms in aliphatic hydroxyl groups of the lignin models, including α-OH and γ-OH. OS represents the three ether-like oxygen atoms of lignin, including oxygen atoms from methoxy groups and the β-O in the β-O-4 linkage. OP stands for the oxygen atom from the aromatic hydroxyl group of lignin. The second way for oxygen atom classification is to elucidate the impact of cleavage of lignin interunit linkages on hydrogen bond interactions between a DES and lignin, where oxygen atoms (or hydroxyl groups) of lignin are divided into four types: α-OH, γ-OH, β-O, and Ar-OH. The first three types are based on the carbon atoms in the aliphatic chain of lignin. Each Adler lignin molecule includes seven α-OH, ten γ-OH, five Ar-OH, and seven β-O, while each GG lignin has one of each type of oxygen atom.

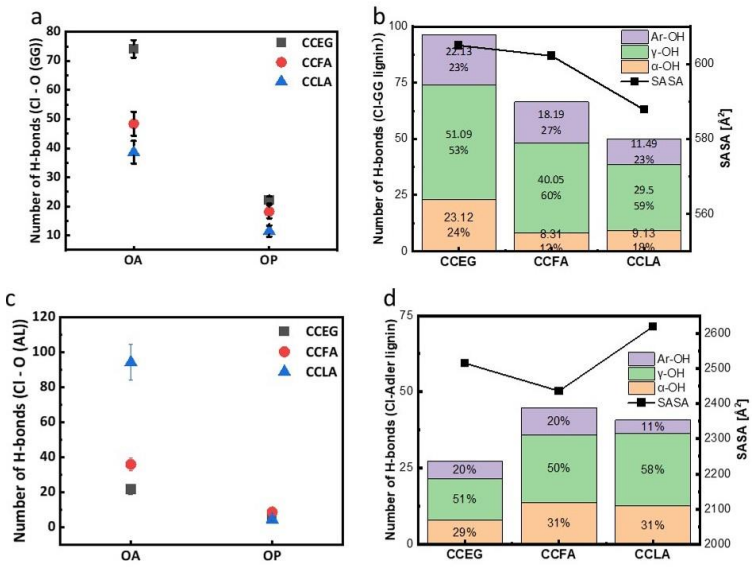

Figure 4.9. Number of H-bonds of chloride–lignin at 300K. GG (a, b) and Adler lignin (c, d).

To find out the preferential sites in lignin for chloride anion to interact with in a DES, Figure 4.9 gives the number of H-bonds between oxygen atoms of lignin molecule and chloride anion of DESs at 300 K. There are two features of interaction between the anion and the lignin: a large part of the ions would accumulate around the aliphatic hydroxyl groups in the lignin, especially around γ-OH; the strength of the interaction is affected by the molecular size of lignin models and other molecules in the systems. The preference on γ-OH is consistent in all the six simulations. In the interaction with GG lignin molecules, more than half of the anions form H-bonds with γ-OH in GG, which also shows a correlation with the average SASA of the lignin molecules (Figure 4.9b).

We deduced that this optimal site within lignin for the anion to interact with in DES is an important clue to find out the role of chloride anion in DES pretreatment in light of how chloride anion functions in IL pretreatment. In a DFT study of the dissolution of GG lignin in ILs, Y. Zhang et al. (2017) found that the optimal site in lignin for the interaction with chloride anion is α-OH. In their later study (Zhang et al., 2019), they

further confirmed that the dehydration of α-C-OH was favored by ionic liquid as the reaction route of lignin hydrolysis in their simulations. The optimal site in IL is different from that in DES for the ions, which means the chloride in DES would have different reaction route or even different role in lignin dissolution. Also, though peaks are also found in the Cl–OA RDF for two lignin model systems within the H-bonds cutoff distance in this work, such peaks are less intense and farther than those in ILs (Zhu et al., 2017). The HBDs should be responsible for the different performance of the anion in DES and IL because the HBD with more strongly electronegative atoms (O) would compete with the anion when interacting with the hydroxyl groups in lignin in DES. HBDs–Cl^- interaction outcompetes anion-lignin interaction, which leaves less opportunity for the anion to interact with lignin molecules. Meanwhile, the anions would also form H-bonds with HBDs, which further restrict themselves from bounding to lignin via H-bonds. Therefore, the anion's role might change from being responsible for the lignin dissolution in IL to other functions. Also, the role of choline chloride might have a strong correlation with the HBDs, which means that although the optimal sites of lignin for the anion are the same in three DESs in simulations, the causation of this preference on γ-OH is different in three DESs and only can be identified after understanding the role of HBDs in lignin dissolution or lignin fractionation.

For the second feature of the interaction between the anion and lignin, it is found that the strength of the anion’s interaction with Adler lignin becomes weaker than that with GG lignin. To have a direct comparison on how the anion interacts with lignin, we normalized the effect of different amounts of the four types of oxygen atoms in Adler lignin by calculating the average H-bonds per oxygen atom for α-OH, γ-OH, and Ar-OH.

For CCEG–Adler lignin systems, each α-OH, γ-OH, and Ar-OH would have 0.0627, 0.0764, and 0.0612 H-bonds averagely. The H-bonds between the anion and lignin is even reduced by 73%, and the anion's preference on γ-OH also becomes less obvious compared to that in GG lignin. The anion does not have enough power to interrupt the intramolecular H-bonds in lignin, and thus its role in lignin dissolution is likely determined by the interaction of HBDs with lignin and anion itself. Specially, the interaction between the HBD and lignin might determine whether the intermolecular H-bonds within lignin can be disrupted significantly and whether the anion can access more hydroxyl groups, especially γ-OH in lignin. The interaction between the HBD and the anion might determine the number of free anions left in the solvent and not being occupied by HBD molecules. The effects of the HBDs on various molecular interactions were further discussed in the latter sections.

4.3.5 Interactions between HBDs and lignin

For most DESs, the most common HBA is choline chloride while HBDs are diverse (Xu et al., 2021). The selection of HBD is rather decisive for lignin dissolution as it can play a key role in interacting with the hydroxyl groups of lignin (Ji & Lv, 2020). An HBD with more than two oxygen atoms tends to have stronger interactions with lignin when we compare the H-bonds in CCLA to that in CCFA or CCEG. Among the three types of oxygen atoms in lignin, OA is the site forming the strongest hydrogen bonds with the HBD in any of the three DESs (Figure 4.10a&c), which is similar to OA–anion interactions (Figure 4.9a&c). For OP and OS, the CCFA and CCLA systems show similar amounts of H-bonds between carboxylic acids and lignin. However, CCEG shows that the H-bonds for the OP site of GG lignin are twice than that found in CCFA and CCLA.

The possible explanation is the formation of [Cl (EG)]$^-$ complexes in CCEG as discussed in the latter sections.

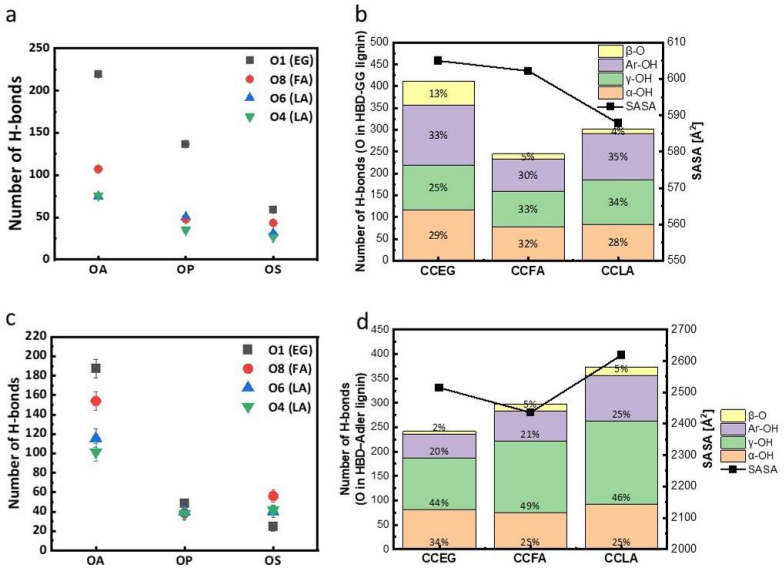

Figure 4.10. Number of H-bonds of O in HBD–lignin at 300K. GG (a, b) and Adler lignin (c, d).

On the other hand, it was found that lignin with different chemistry can form different H-bonds in a DES when comparing GG and Adler lignin. As depicted in Figure 4.10b&d, the number of H-bonds in the HBD-GG interaction at 300 K follows the order CCEG > CCLA > CCFA for GG lignin and CCLA > CCFA > CCEG for Adler lignin. The decrease in H-bonds between CCEG molecules (either chloride anion or ethylene glycol) and lignin molecules when interacting with Adler lignin indicates that CCEG is not an efficient solvent in the dissolution or depolymerization of Adler lignin. The affinity of CCFA and CCLA is stronger for their interaction with Adler lignin than GG lignin. The different associations between DES–lignin in the simulated systems should relate to the capability of a DES to deal with inter-/intra-molecular H-bonds in lignin molecules, which can determine DES effectiveness for lignin dissolution and depolymerization. While lignin dissolution focuses on having strong hydrogen bond

interactions between a DES and lignin molecules to avoid lignin agglomeration, lignin extraction often involves the interruption of interunit linkages in lignin by a DESs. In other words, DES having excellent lignin solubilization may not necessarily ensure their performance on lignin extraction, and vice versa. For example, the experimental study showed that increasing the amount of ChCl in CCLA can improve lignin extraction from biomass, but decrease lignin solubility in the DES (Smink et al., 2019).

Comparing the total H-bonds of chloride–lignin interactions and HBD–lignin interactions in all the three DES, we can have a general perception that HBDs play an important role in the hydrogen bonding interaction with lignin molecules regardless of the size of lignin model compounds. A similar finding was reported for the interaction between CCLA and another lignin dimer, veratrylglycerol-b-guaiacyl ether (VG) (Ji & Lv, 2020). Similar to the anion, HBDs also have their own preferential interacting sites in lignin. During lignin extraction, HBDs would be pre-positioned around the linkages of lignin (probably in their preferential sites) for the further hydrolysis reaction. The β-O-4 bond of lignin is always considered the most vulnerable intermolecular linkage in lignin (Boerjan et al., 2003). The mechanism for the cleavage of β-O-4 bonds is proposed to involve three primary steps: (1) the hydroxyl group (α-OH or γ-OH) would be eliminated; (2) the carbon atom initially linked with the hydroxyl group then would be deprotonated; (3) the hydrolysis of the β-O-4 bond would be finished with the removal of water molecules (Zhang et al., 2019). Therefore, the role of HBD here should provide protons to attack the hydroxyl groups in the β-O-4 bond, which would further cause the elongation of the C-O bond. Based on the average H-bonds for each oxygen atom in lignin molecules (Figure 4.10b), HBD shows different strengths to attack the α-OH and

γ-OH. Ethylene glycol molecules attack α-OH more frequently, the proportion of H-bonds with α-OH (35.5%) in Adler lignin is even larger than that with GG lignin (29%). Formic acid and lactic acid form more H-bonds with γ-OH, and the number of these H-bonds further increases when encountering Adler lignin. The proportion of average H-bonds per oxygen atom for γ-OH is 36.6% for formic acid and 32.9% for lactic acid. The ratio of H-bonds with α-OH to H-bonds with γ-OH is 1:1 for GG lignin and 7:10 for Adler lignin. The number of H-bonds of O in HBD with γ-OH increased dramatically in CCFA (by 80.3%) and CCLA (by 68.5%) when it comes to interaction with Adler lignin, but it only increased by 3% in CCEG. Such increase for CCFA and CCLA reveals the importance of the amount of γ-OH in lignin on the interaction between the lignin and DESs.

The propensity of HBDs for interacting with the hydroxyl groups of lignin might relate to the complexes formed in the solvents. As mentioned previously, carboxylic acid dimers appear in CCFA and CCLA, while $[Cl\ (EG)]^-$ complex is more common in CCEG. Two major differences among the complexes in the three DESs are the supramolecular size and available protons. For carboxylic acid dimers, they have more protons available than the $[Cl\ (EG)]^-$ complex, and the protons from carboxyl groups can easily dissociate from the dimers. However, the carboxylic acid dimers, especially lactic acid dimers, with larger supramolecular size than the polyol complexes, might occlude oxygen atoms on carboxylic acids prevailing their interactions with the hydroxyl groups in lignin. In general, γ-OH is far away from the aromatic rings of lignin than α-OH and β-O, making it more accessible to the carboxylic acid dimers, especially for Adler lignin.

In GG–DES systems, GG molecules would be stretched via H-bonds by the

surrounding solvent molecules and the other GG molecules. However, it seems difficult to analyze how the structural change in Adler lignin is governed by the molecular interactions because Adler lignin has more branches and complex structure. Therefore, we further visualize how the anion and oxygen atoms in HBDs surround the GG molecules with the spatial distribution function (SDF) centered on GG lignin. The purpose is to analyze how the optimal sites in GG for the HBD and the anion would determine the openness of GG structure. The favorable sites for H-bonding with chloride anion (green) and the oxygen atoms of HBDs (purple and cyan) around GG lignin are shown in Figure 4.11. The chloride anions in three DESs are mainly surrounding the hydroxyl groups of GG lignin, which is consistent with the calculated coordination numbers and number of H-bonds in Figure 4.9a&b.

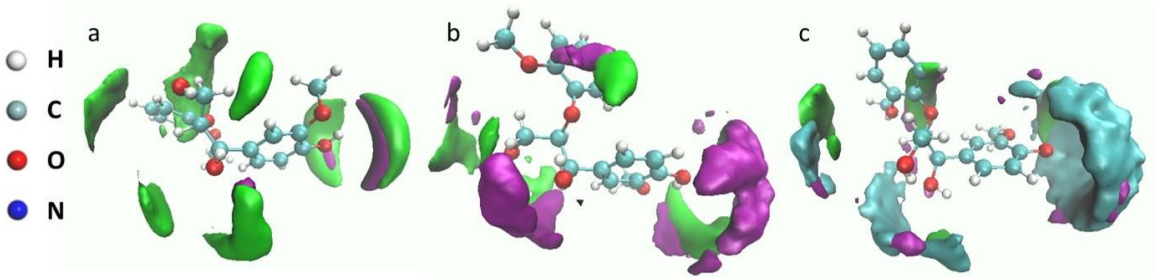

Figure 4.11. Spatial Distribution Function (SDF) of chloride anion (green) and oxygen atom of HBD centered around GG lignin. (a) CCEG, (b) CCFA, (c) CCLA. Isovalue for all chloride anion is 3g/cm^3 and isovalue for all oxygen atom is 1.6g/cm^3. O1, O4, O8 in purple, O6 in cyan.

The accumulation patterns of HBD around the GG lignin show strong correlations with the HBD–HBD and HBD–anion interactions that are the common complexes in a DES. For CCEG, the spatial distribution area for the oxygen atoms of ethylene glycol overlaps with the area occupied by the anions in CCEG. Such overlap can also be found in the SDF centered on choline cation of pure CCEG, as shown in Figure 4.11a, which is an evidence for forming a massive amount of [Cl (EG)]$^-$ complexes in the CCEG.

Therefore, instead of interacting directly with individual ethylene glycol molecules, GG lignin is more likely to interact with these complexes. These complexes in high density appear around the OP in GG, which is corresponding to the significant H-bonds found between OP and O1 in Figure 4.10a. The strong hydrogen bond interaction between Ar-OH and the complexes can stretch the GG molecules to an extended structure. The appearance of $[Cl\ (EG)]^-$ complexes around the α-OH can also be observed in Figure 4.11a. Compared to CCEG, oxygen atoms in HBDs of CCFA and CCLA are mainly accumulated around γ-OH and Ar-OH. The proportion of H-bonds formed with Ar-OH, α-OH, and γ-OH is not significantly different, and only the H-bonds with γ-OH is slightly more than those with the other two hydroxyl groups in GG (Figure 4.10b). It indicates that the hydrogen boding strength on those three sites should be comparable and the stretching effects on the GG molecules should be similar. However, the average SASA of GG is much smaller in CCFA than in CCEG and CCLA. The arrangement of the HBDs might be responsible for such a difference. In CCFA, both the anion and O8 in formic acid show the same direction around the OP, but do not overlap with each other. This arrangement allows the other GG molecules to form intermolecular H-bonds and these H-bonds would benefit to an opener structure of GG. However, in CCLA the OP in GG is mostly covered by O6 in lactic acid, leaving GG molecules less opportunity to contact with each other. Thus, GG might tend to self-aggregate to a folded structure. Such arrangement is not good at the extension of GG lignin or lignin with small molecular size, but it is indeed good for a larger lignin molecule with more branches, such as Adler lignin in this study (Figure 4.10d) because the solvent complexes can be imbedded into the void of the branches and prevent different branches from interacting with each other.

4.3.6 Interactions between DES and lignin–cellulose bulk

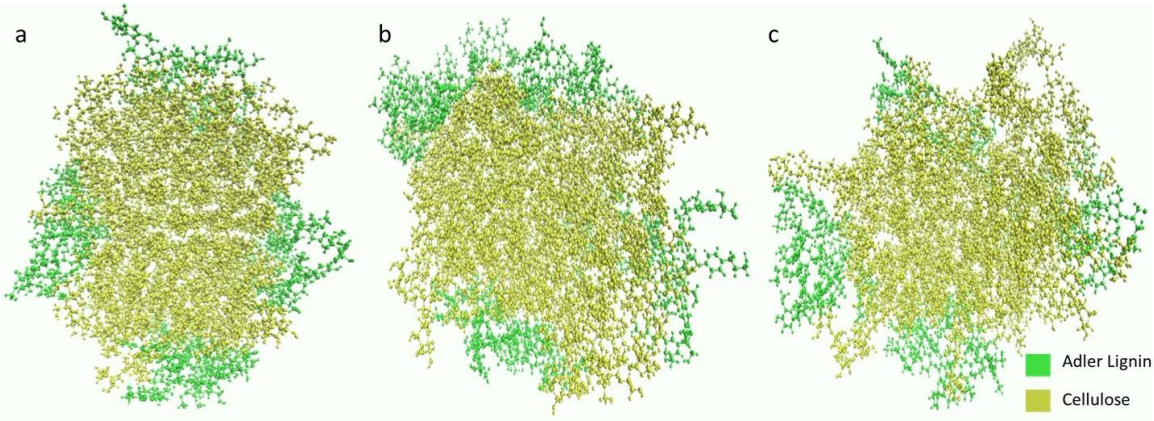

Figure 4.12. Visual diagrams of the final configurations of lignin-cellulose bulk in (a) CCEG, (b) CCFA, and (c) CCLA.

The simulations of interaction between DES and lignin–cellulose bulk were aimed to reproduce the adsorption process and see how the solvent can affect this adsorption. Figure 4.12 shows the snapshots of how lignin was finally attached on the surface of cellulose bulk. The adsorption of lignin and cellulose is primarily driven by either hydrogen bonding interactions between lignin and cellulose surface or the orientation of the stacking structure between aromatic rings and the glucopyranose ring of cellulose. Thus, two main aspects were considered to monitor changes in the adsorption process, namely the number of hydrogen bonds and number of close contacts. Figure 4.9a shows the number of H-bonds for three pairs of interaction including lignin–lignin, lignin–HBD, and lignin–cellulose. For H-bonds between lignin and HBD, lactic acid shows the most intense hydrogen bonding with lignin, followed by ethylene glycol and formic acid. In contrast, H-bonds in both lignin–lignin and lignin–cellulose follow the order CCEG > CCFA > CCLA. This further confirms that hydrogen bonding between HBD and lignin can interrupt the intramolecular hydrogen bonding network of lignin. The number of H-bonds for lignin–cellulose is roughly equal to the H-bonds for lignin–lignin in CCEG

and CCFA, but it is smaller in CCLA. These results indicate that there is competition among cellulose, HBD, and lignin when it comes to the formation of H-bonds. H-bonds in lignin–lignin and lignin–cellulose are apparently dominant in all the three DESs at 300K, which can relate to the recalcitrance of lignocellulosic biomass. However, different HBDs can reduce these two types of H-bonds in various degree. For example, our simulation revealed that lactic acid can reduce most of H-bonds in biomass. Comparing the H-bonds in CCEG and CCFA, formic acid is not as active in hydrogen bond interaction with lignin as ethylene glycol, but it still works better to interrupt the hydrogen bond network in this lignin–cellulose bulk.

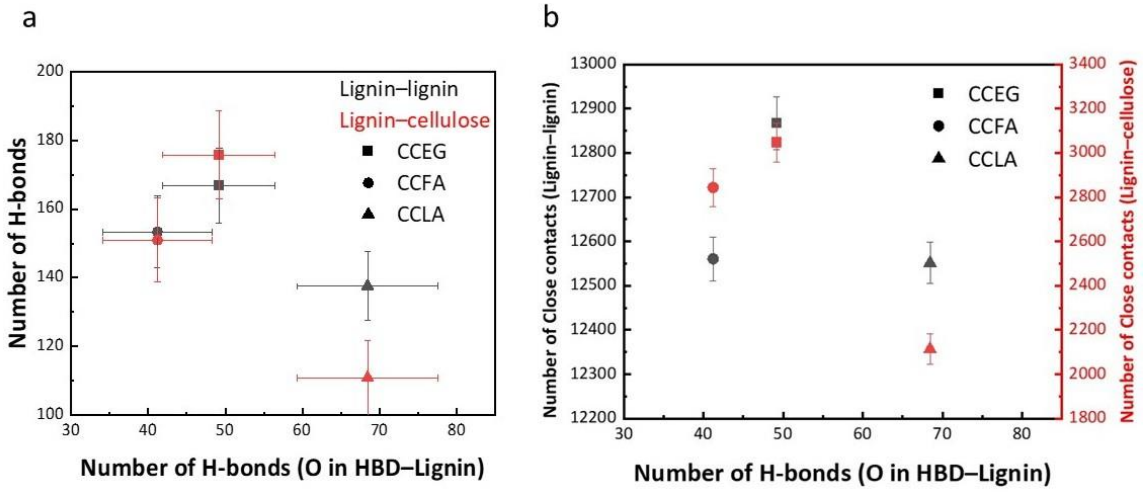

Figure 4.13. The correlation of (a) number of H-bonds and (b) close contacts of lignin–lignin (black) and lignin–cellulose (red) with the number of H-bonds in HBD–lignin.

Atom–atom close contact of lignin–lignin and lignin–cellulose was also calculated for further elucidation of the changes of distance between lignin and the surface cellulose (Figure 4.13b). The reduced number of close contacts between atoms of lignin–cellulose in CCLA confirmed the ability of lactic acid to weaken the H-bonds between lignin and cellulose. Although formic acid does not show a similar ability to disrupt the lignin–cellulose interactions, it has a comparable strength with lactic acid to reduce close contact

of atoms within lignin.

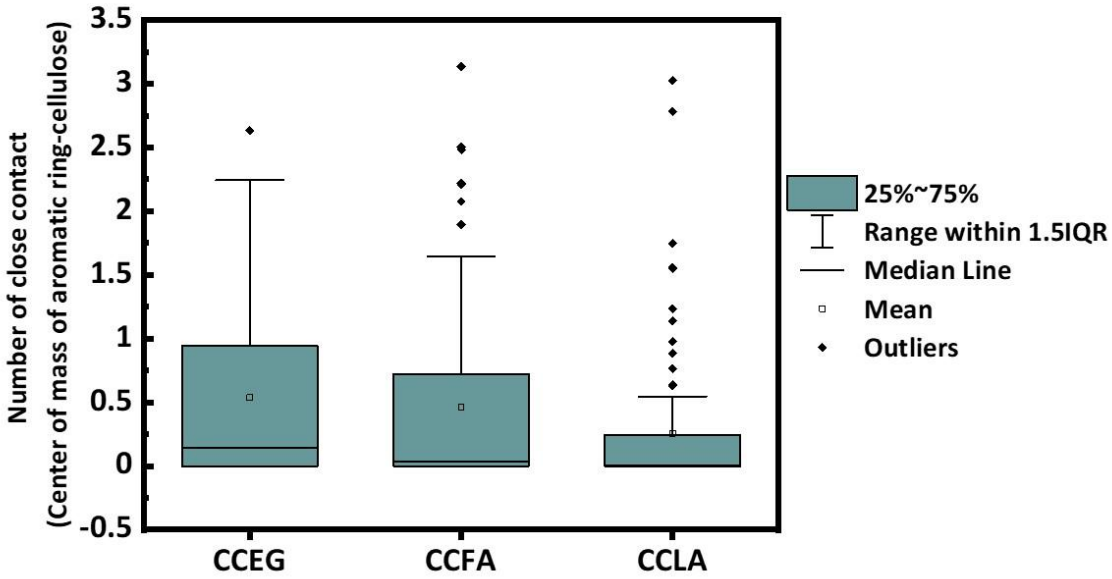

Figure 4.14. Average number of close contact of center of mass of aromatic ring to atoms of cellulose in different DESs.

As surface chemistry of cellulose is another factor influencing its affinity to lignin, we also investigated how a DES would interact with lignin on different surfaces of cellulose. Figure 4.14 shows the average number of close contacts of the center of mass (COM) of the aromatic rings in lignin bounded to the surface of cellulose. The percentage of aromatic rings (out of 96 in total for simulation) which has no close contact with any atom of cellulose is 28%, 38.5%, and 50% in CCEG, CCFA, and CCLA, respectively. Moreover, lignin–cellulose close contacts and the close contacts on either the hydrophobic or hydrophilic surface of cellulose were considered separately (Figure 4.15). The initial geometry depicts how Adler lignin molecules are placed on selected surface of cellulose (Figure 4.15a). In CCEG, lignin does not show obvious preference to a hydrophobic or hydrophilic surface of cellulose. In contrast, preferential bindings of lignin to the hydrophilic surface of cellulose are found in both CCFA and CCLA, which

was reflected by a reduction in the number of close contacts of lignin-cellulose. Among all the three HBDs, lactic acid not only interrupts the intra- or inter-molecular hydrogen bond networks of lignin, but also works best to reduce lignin-cellulose contacts on the hydrophobic surfaces and gives the narrowest distribution of average close contact of COM of aromatic rings with cellulose's hydrophobic surface (Figures 4.14&15). Formic acid is not as strong as lactic acid in forming H-bonds with lignin to reduce lignin-cellulose contact on the hydrophilic surface, but is still able to reduce lignin–cellulose contact on the hydrophobic surfaces of cellulose and to impede the self-aggregation of lignin. Compared to carboxylic acid-based DESs, CCEG shows less potential in disrupting the adsorption between lignin and cellulose even though it might form more H-bonds with lignin.

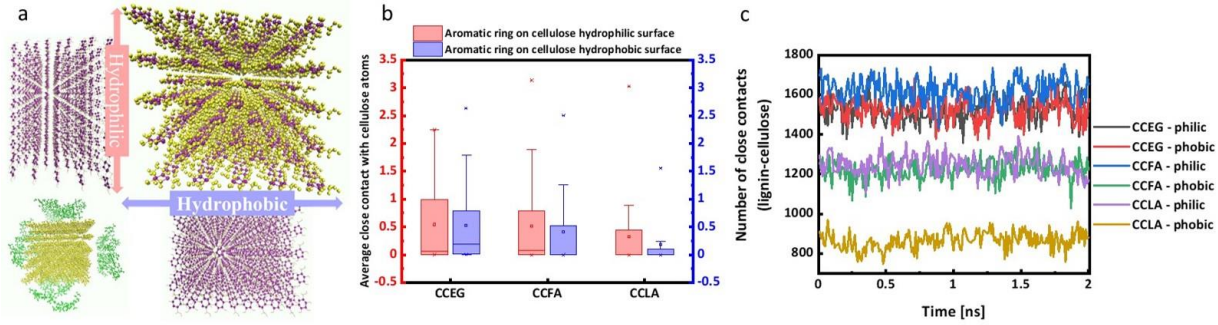

Figure 4.15. (a) Diagram of hydrophilic and hydrophobic surface of cellulose. (b) Average number of close contact of center of mass of aromatic ring to atoms of cellulose on either hydrophilic or hydrophobic surface in different DESs. (c) Number of close contact of lignin-cellulose on either hydrophilic or hydrophobic surface in different DESs.

Based on this comparison of close contact of lignin on both hydrophobic and hydrophilic surfaces of cellulose, we concluded that DESs are able to disturb the redeposition of lignin on cellulose surfaces especially on the hydrophobic surface, by reducing the occurrence of restricted aromatical ring structures in lignin on the cellulose's hydrophobic surfaces as well as by competing with cellulose via stronger hydrogen

bonding. In prior studies concerning theoretical investigations of cellulose-lignin associations (Besombes & Mazeau, 2005a, 2005b; Lindner et al., 2013), such associations in explicit water are obviously observed in the hydrophobic surfaces. The opposite results between explicit water and DES show two different behaviors of lignin in a poor solvent and in a good solvent. In a good lignin solvent, lignin can be efficiently detached from the cellulose hydrophobic surface and thus removed into the liquid phase. Among three DESs, CCLA results in the most aromatic rings of lignin dissociating from the cellulose hydrophobic surface following by CCFA and CCEG.

4.4 Discussion

This study used bulk phase all-atom MD simulations to elucidate the solvent structure of three choline chloride based DESs and the structure of two types of lignin models at those DESs. The atomic-level details of the interaction within the solvents as well as between solvents and lignin are readily resolved from MD simulations. Lignin structure was characterized by average solvent-accessible surface area distribution, radius of gyration distribution and lignin–lignin hydrogen bonds. As for the interactions between solvent and lignin, it was described via lignin–DES hydrogen bonds, radial distribution function and spatial distribution function calculations.

The calculations mentioned above demonstrate the predominant impact of HBD on the solvent structure and lignin conformation. This discussion will be divided into three parts: Different types of complex formed and determined by HBD; HBD complex is the local solvent of lignin and is pre-positioned around linkages of lignin for hydrolysis process; HBD can efficiently weaken lignin absorption on cellulose surface, especially on hydrophobic surface.

4.4.1 Role of HBD in DES complex formation

From the calculation of the radial distribution function, hydrogen bond numbers, and the spatial distribution function, it is clear that the choice of HBD in DES strongly affects the local molecular arrangement. A straightforward observation is the total number of H-bonds available in the solvent. When a HBD has more oxygen atoms per molecule, the hydrogen bond network of the DES tends to be denser (see supporting information) as more H-bonds are generated in HBD–HBD and HBD–anion interactions. In CCEG, H-bonds are mainly from the HBD–anion interactions, while in CCFA or CCLA, H-bonds are mainly contributed by HBD–HBD interactions. In the two carboxylic-acid-based DESs, aggregation is found among the carboxylic acids, which leads to weaker interactions between chloride anion and the HBD. Under this circumstance, only small amounts of chloride anion are able to approach the acid. At the same time, the diffusion of most of the anions would be slow down by carboxylic acid complex, and remain bound to choline cation, either via hydrogen bonding with hydroxyl groups, or via electrostatic forces with nitrogen atoms. Similar conclusions were mentioned in another study(Perkins et al., 2014), in which chloride anion was found to have intense hydrogen bonding with choline cation in choline chloride/malonic acid DES. Consequently, two different types of complex structures are formed in polyol based DESs and carboxylic acid based DESs. A $[Cl\ (EG)]^-$ complex is prevalent in CCEG solvent, while a carboxylic acid dimer is predominant in both CCFA and CCLA solvents. This complex assumption can be also reflected in the unique distributions in spatial distribution function centered around choline cation (Figure 4.7). Overlap was found in distribution of chloride anion and ethylene glycol, while an interlaced distribution was observed for chloride anion and

carboxylic acid.

4.4.2 Role of HBD and Chloride in lignin dissolution

There are two aims of using two lignin models: 1) finding out whether the particle size of lignin model would affect the hydrogen bond interaction between DES and lignin in the simulation; and 2) identifying the distinct features for three DESs in the interaction with lignin. To characterize the lignin structural changes, SASA values and number of lignin-lignin hydrogen bonds are used as reference and both parameters has been used to characterize lignin structure in other studies(Lindner et al., 2013; Smith et al., 2016). For the first aim, it was found that for a lignin dimer model, the main lignin–lignin interaction is intermolecular interaction, which means the openness of a lignin molecule is affected by the solvent and other lignin molecules at the same time. Because the relatively smaller size and larger mobility compared to Adler lignin, GG lignin dimer is more flexible in the solvent and has higher probability to have inter-lignin-lignin contacts. Thus, the SASA of GG would change upon the influence of H-bonds from solvent molecules and from other GG molecules, and it is hard to tell directly how the interaction with a solvent would change lignin structure. Also, when finding out the preferential site in lignin for solvent molecules to bind to, it might be difficult to tell the optimal sites, as all oxygen atoms in dimer lignin are easy to approach. However, an advantage of using GG model is allowing us to have a straightforward observation of the local molecular arrangement of solvent molecules around the β-O-4 linkage in lignin. As for Adler lignin, a lignin model with more branches, larger particle size and more types of linkages, the intramolecular H-bonds are more common within such lignin model. When interacting with solvent molecules, large steric hindrance in Adler lignin might impede solvent molecules from

hydrogen bonding with all the oxygen atoms in lignin. Because of that, the optimal site for solvent molecules to bound with become more obvious to observe. Besides, once the solvent molecules bound to the hydroxyl groups in lignin, they might be able to self-position in lignin molecules and prevent lignin molecule from aggregating via intra-molecular H-bonds.

For the second goal, via combining the observation on GG and Adler lignin, we found that the choice of HBDs would determine the way that DES would interact with lignin and also the role of the anion during lignin dissolution or fractionation in the form of a complex structure. The role of HBD is likely to be to provide the protons necessary for lignin hydrolysis by hydrogen bonding with hydroxyl group in the linkage of lignin. Then the size and the composition of HBD complex would determine the amount of hydrogen bonds formed with the lignin and the optimal sites in lignin for interaction. Although the reaction routes for DES to fractionate lignin has not yet clear, we might refer to the relative study of ionic liquid as the two solvents have similar physical properties. In the study of β-O-4 bond cleavage by the sulfonic-acid-functionalized ILs, Zhang et al. (2019) carried out three potential routes for this cleavage, dehydration of α-C-OH, dehydration of γ-C-OH, and protonation of β-O, and the molecules to execute the cleave is "Zwitterion/H_2SO_4 complex". Another ILs applied in lignin dissolution also have chloride anion in the solvent, which might provide more inspiration on this choline chloride-based DES study. In an IL, chloride anion is usually found to interact preferentially with the hydroxyl groups of lignin (Zubeltzu et al., 2020) because an anion could have high hydrogen bond basicity that favors hydrogen bond interactions with hydroxyl groups in lignin and then further breaks up the lignin's intramolecular hydrogen

bond network.(Moyer et al., 2018) The impact of the anion is essential to determine the lignin solubility of a ionic liquid (Zakzeski et al., 2010) and the reaction route to cleavage the linkages of lignin, leading to various degrees of lignin structural modification.(George et al., 2011) Based on the above ILs delignification mechanism studies, we would know the two prerequisite in lignin bond cleavage of DES should be a good HBD/HBA to interact with lignin and a complex formation among the constituents in DES which probably would stabilize the proton transition process. Presumably, DES might also cleave lignin linkages via one or more similar paths to dehydration of α-C-OH, dehydration of γ-C-OH, and protonation of β-O.

The different performance of polyol DES and carboxylic DES in biomass pretreatment have been found in experiments. For example, without additional water or acids, the lignin removal rate in CCEG can be much lower than CCLA(Chen et al., 2018a; Chen & Wan, 2018) in switchgrass pretreatment. Besides, the local arrangement of chloride anion might also vary in CCEG and CCLA. In CCEG, ethylene glycol molecules preferentially occupy around the α-OH in lignin which is the same site for chloride anion to occupy in ILs(Y. Zhang et al., 2017). The same favorable site in lignin indicates that the $[Cl\ (EG)]^-$ complex with most of the hydroxyl groups being occupied by the anions, is more likely to accept the protons from lignin in the hydrogen bond interaction. Therefore, the $[Cl\ (EG)]^-$ complex might cleave β-O-4 bond through the dehydration of α-C-OH, which requires further investigation. Also, there might be an atom exchange between the complex and the lignin. When the α-OH fall off from lignin due to the interaction with the complex, the chloride anion from the complex might bound to the α-C immediately. In a study of the role of chloride anion in CCEG, Zhu Chen et al. (2020) compared the

extracted lignin from the CCEG pretreatment with a different molar ratio of HBD/HBA. They proposed that the role of the anion is to stabilize the α-C in β-O-4 linkage after α-OH being removed in DES pretreatment. With the anion's protection, the extracted lignin would preserve more β-O-4 linkages after the pretreatment. This proposed mechanism means that some of the anions would stay around the lignin and as soon as the hydroxyl groups in the β-O-4 linkages are removed by HBDs, and the carbocation appears, they are able to bound to the carbocation quickly to stop the cleavage of β-O-4 bond. Our finding of the complex here further confirms the feasibility of the anion binding to α-C and the role of the anion to preserve β-O-4 bond.

In contrast, in two carboxylic acid-DESs, the carboxylic acid dimers appear and based on the count of H-bonds in Figure 4.10d, the dimers should mainly surround the γ-OH in lignin. The features of such dimers are that they can either provide or accept protons in the hydrogen bond interaction with lignin molecules. The hydroxyl groups in lignin might be trapped within the dimer and will be blocked from contacting with other oxygen atoms in lignin. Such dimers, especially the lactic acid dimers, have a larger particle size and thus tend to interact with the hydroxyl groups with less steric hindrance effect, such as γ-OH and Ar-OH. Because both carboxylic acid molecules and the anions have the same optimal sites in lignin, they might cooperate with each other to remove the γ-OH from the linkage. In a recent experimental study of using CCLA for biomass pretreatment, Smink et al. (2019) found that the existence of the anion would accelerate the delignification rate of lactic acid, but would not increase the lignin solubility of the solvent. Our simulations reveal the possible mechanism behind their experimental observation that is joint interaction on the same site in lignin with the HBDs result in

accelerated delignification process.

Compared to formic acid dimer, lactic acid dimer shows its own advantages, which is capable to form more hydrogen bonds as shown in Figure 4.b, c. The arrangement of lactic acid complex might do a better job on blocking the formation of intrapolymeric hydrogen bonds with its large coverage around the hydroxyl groups of lignin. Also, it is interesting to find that when the carboxylic acid forms less H-bonds with lignin, the chloride anion in this solvent would have more H-bonds with lignin. Chloride anion and the carboxylic acid would compete with each other for interacting with lignin, and under such competition, the hydroxyl groups in lignin would face with more intense hydrogen bond interaction and become easier to drop off from the linkage. Furthermore, the above observations confirm the role of HBD complex as the medium to reduce tendency of lignin-lignin or intra-lignin interaction, as well as the main source of proton donor in the cleavage of lignin linkage

4.4.3 Impact of HBD in the adsorption between lignin and cellulose

While blocking the hydrogen bond within lignin is the main task in lignin dissolution, detaching lignin from cellulose surface is another task for DESs when pretreating lignocellulosic biomass. The lignin-cellulose adsorption process was found to be surface-dependent. On the hydrophilic surface of cellulose, the adsorption seems hydrogen bond-driven, which means HBDs have to provide more oxygen atoms/hydroxyl groups so that they can compete with the hydrogen bonds between cellulose and lignin. An ideal HBDs would be able to bind with as many oxygen atoms in lignin as possible to weaken the hydrogen bond interaction between lignin and cellulose as well as the H-bonds within lignin. Then lignin can be detached from cellulose surface and would not

have self-aggregation after the detachment. Therefore, CCLA is more advantageous in such missions as it can disrupt the greater number of H-bonds of lignin-cellulose and that of lignin-lignin compared to the other two DESs. CCFA was found to have a reduction on lignin–lignin close contacts comparable with CCLA. Because of that, the lignin structure in this solvent becomes more open, which can be confirmed through the comparison of average SASA of Adler lignin, following the order as CCFA (2541.98 $Å^2$) > CCLA (2426.74 $Å^2$) > CCEG (2316.53 $Å^2$). However, a great number of lignin–cellulose close contacts on the hydrophilic surface is observed in CCFA (Figure 4.11c). This phenomenon implies that although CCFA is able to prevent lignin from aggregating, it does not provide competitive H-bonds to separate lignin from cellulose. In contrast, the consequence of a more open lignin structure in this solvent can facilitate the lignin-cellulose hydrogen bond interaction on the hydrophilic surface as the contact area becomes larger.

On the hydrophobic surfaces of cellulose, most of the area is covered by the glucopyranose rings, so hydrogen bonding is no longer the dominant force to attract lignin. It is consequently more favorable for lignin to bind to the hydrophobic surfaces of cellulose within some poor solvents (e.g., water) (Vermaas et al., 2019). When it comes to DESs which are better solvents for lignin than water, this affinity is dramatically reduced. In all the three DESs, no preference of close contact was found between lignin and cellulose on the hydrophobic surface. In DES, it is no longer necessary for lignin to increase the contact area with the hydrophobic surface to avoid contact with the solvent molecules as it does in water. Thus, the propensity for aromatic ring to stay parallel to the hydrophobic surface (Besombes & Mazeau, 2005b) is also reduced. In Figure 4.11b, the

close contact of the COM of aromatic ring on hydrophobic surface is even smaller than those on hydrophilic surface. As a consequence, the DES is better at removing lignin from cellulose surface via hydrogen bonds than water.

4.5 Conclusions

This MD simulation study reveals the local molecular arrangements for three common DESs and characterized the structural changes of lignin and association of cellulose-lignin in the DESs. The three DESs comprise choline chloride as an HBA paired with ethylene glycol, formic acid, or lactic acid as an HBD. We found that an HBD plays a dominant role in the solvent structure as it forms different types of complexes with anion and other HBD molecules depending on the nature of the HBD. The HBD-based supramolecular complexes can further affect the solvation of lignin by changing the density of the hydrogen bond network of DESs as well as by limiting lignin–lignin hydrogen bonds. The efficiency of lignin solvation mainly depends on the size and functional groups of HBD complexes. Meanwhile, the HBD complexes were found to have different preferential sites on lignin. These mechanisms should account for different performance of DESs on lignin dissolution and extraction. The mechanistic insights obtained from this MD simulation would provide guidance on the rationale design of DES for biomass pretreatment, lignin extraction, and lignin valorization toward sustainable pulping and biorefining.

.

CHAPTER 5

CONCLUSIONS AND FUTURE WORK

Deep eutectic solvents (DESs) are promising solvents for applications such as biomass pretreatment and lignin upgrading. The outstanding features of DESs include no or little toxicity, biodegradability, and thermally stability, etc. Tailorability of DES properties with different combinations of hydrogen bond donor (HBD) and hydrogen bond acceptor (HBA) is particularly interesting for lignin dissolution given heterogonous and complex nature of lignin. The MD simulation study in this thesis enables us to gain mechanistic insights into the interaction of DES constituents and lignin and the effects of such interactions on lignin dissolution behavior. The simulation findings have implications on separating lignin from lignocellulosic biomass using rationally designed DESs to produce cellulose-rich pulp and quality technical lignin for multi-purpose biorefining.

Exploiting polarized force field which is able to include the charge delocalization occurring between the anion and HBD for higher accuracy of the DESs simulation is one of the main challenges for DES simulations, as it would possibly require more simulation time and model development. In biomass pretreatment, the structure of biomass (e.g., lignin structure and chemistry, cellulose, hemicellulose) is another factor determining pretreatment performance. However, since most of the studies about interactions between DESs and lignin were based on simulation with low molecular weight lignin model (e.g., dimer or tetramer), the impacts of the heterogeneity of lignin on the interactions with the solvents might be overlooked. We filled this gap in our study by simulating lignin models with various types of linkages and types of monomer units that better represents native

lignin structure. As the study of DESs is still in its early stages, experiments are still the first and the most convincing choice. Nevertheless, the MD simulation based on phenomena deduced from experimental studies provides a more detailed view of possible mechanisms for lignin dissolution behaviors and structural changes in a DES. The accuracy of MD would also be further improved based on the increased body of knowledge gained from both experimental and theoretical studies.

Based on the discussions above, some prospective research is expected in future. The customized scaled-charge method, depending on the type of HBD, might be a solution to achieve higher accuracy in reproducing the thermodynamic properties of DESs. Besides, lignin recondensation would always happen during the pretreatment, which leads to poor quality of the fractionated lignin, because this behavior would increase the C–C bonds which is hard to break down, and also increase the molecular weight of the fractionated lignin (Wen et al., 2014). Lignin models of different spatial scales, or with different linkages types, or with different amounts of methoxy groups and phenolic groups, should be considered so that the lignin recondensation can be better captured in simulations. Moreover, it can benefit with the studies about the impact of DESs on mitigating such recondensation of lignin, which can probably give better understanding on how to select a proper solvent media to fractionate lignin with an expected structure (e.g., less condensation region, more phenolic groups/β-O-4 linkages being preserved). To assure the reliability of MD simulations in this research area or testify the conclusions derived from the simulation, some strategies can be considered. One is to include some parameters that can quantify the strength of interactions between DESs and lignin and can be assessed by both experiments and simulations. Such

parameters are necessary to know how far the deviation of the simulated data can be compared to reality. The other strategy is to include simulations of the interactions between certain solvents and lignin. Those solvents should have significant lignin solubility based on information from experiments. The difference in interaction strength between interaction of traditional solvents and lignin and that of DESs with lignin should be comparable. The third strategy is to incorporate simulations by more accurate computational methods including DFT and AIMD. By comparing the results from those computational methods, we can tell whether the results from MD can be reproduce and further determine to what degree that we can rely on MD to explore the solvent effects in lignin extraction.

APPENDIX

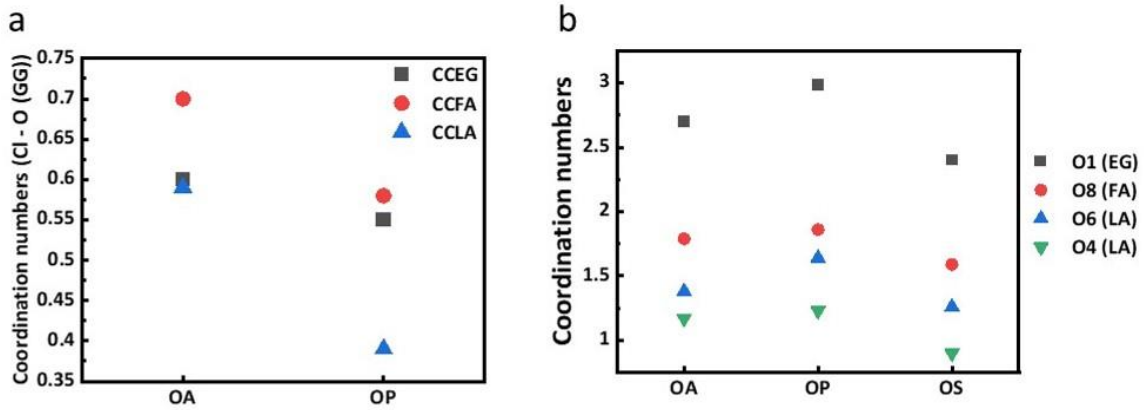

Figure A.1. Coordination number of (a) Chloride–GG and (b) HBD–GG at 300K.

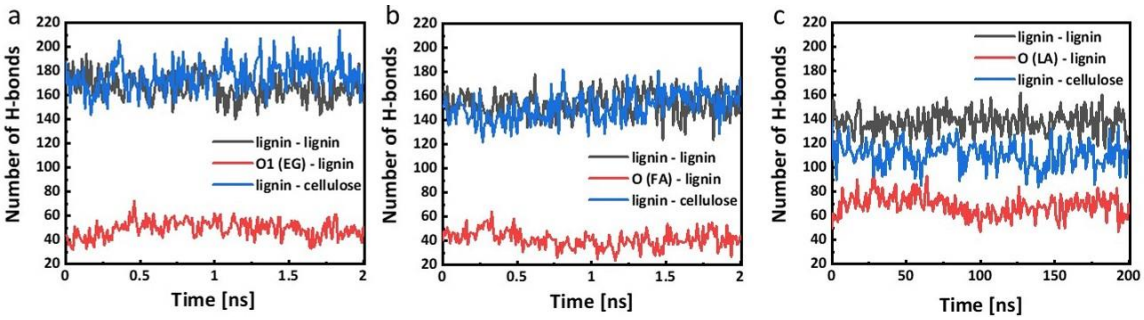

Figure A.2. Number of H-bonds of lignin–lignin (black), O (HBD) –lignin (red) and lignin–cellulose (blue) in (a) CCEG, (b) CCFA, (c) CCLA.

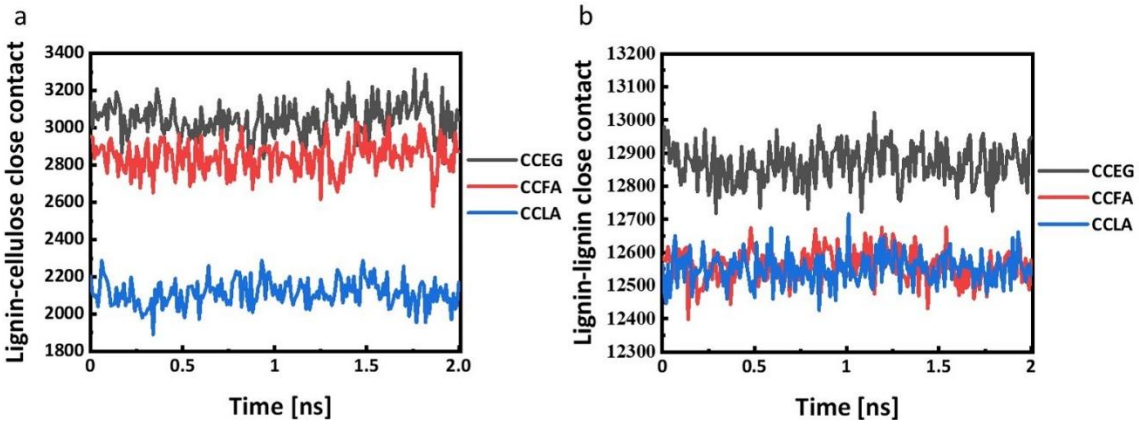

Figure A.3. Number of close contact of (a) lignin–lignin and (b) lignin–cellulose in CCEG (dark), CCFA (red), CCLA (blue).

Table A.1. Average H-bonds per oxygen for each type of oxygen of lignin[a]

	Cl - α-OH	Cl - γ-OH	Cl - Ar-OH	O in HBD - α-OH	O in HBD - γ-OH	O in HBD - Ar-OH	O in HBD - β-O
GGCCEG	23.12	**51.09**	22.13	117.26	101.91	**136.70**	55.15
ALCCEG	7.90	**13.76**	5.51	81.60	**105.68**	48.17	5.93
GGCCFA	8.31	**40.05**	18.19	77.29	**81.32**	74.61	11.43
ALCCFA	13.71	**22.30**	8.76	75.26	**146.59**	61.07	14.34
GGCCLA	9.13	**29.50**	11.49	83.71	101.33	**106.38**	10.78
ALCCLA	12.62	**23.72**	4.46	92.29	**170.78**	93.56	17.37

[a] Numbers in bold means the highest value of chloride anion and oxygen atoms in HBDs among all types of hydrogen bonds with Adler lignin.

Table A.2. Total H-bonds for each type of oxygen of lignin[a].

	Cl - α-OH	Cl - γ-OH	Cl - Ar-OH	O in HBD - α-OH	O in HBD - γ-OH	O in HBD - Ar-OH	O in HBD - β-O
GGCCEG	0.193	**0.426**	0.184	0.977	0.849	**1.139**	0.46
ALCCEG	0.0627	**0.0764**	0.0612	**0.648**	0.587	0.535	0.06
GGCCFA	0.069	**0.334**	0.152	0.644	**0.678**	0.622	0.1
ALCCFA	0.109	**0.124**	0.097	0.597	**0.81**	0.68	0.13
GGCCLA	0.076	**0.246**	0.096	0.698	0.844	**0.886**	0.09
ALCCLA	0.1	**0.132**	0.05	0.732	0.949	**1.04**	0.16

[a] Numbers in bold means the highest value of chloride anion and oxygen atoms in HBDs among all types of hydrogen bonds with Adler lignin.

BIBLIOGRAPHY

Abbott, A. P., Boothby, D., Capper, G., Davies, D. L., & Rasheed, R. K. (2004). Deep eutectic solvents formed between choline chloride and carboxylic acids: versatile alternatives to ionic liquids. *Journal of the American Chemical Society, 126*(29), 9142-9147.

Abraham, M. J., Murtola, T., Schulz, R., Páll, S., Smith, J. C., Hess, B., & Lindahl, E. (2015). GROMACS: High performance molecular simulations through multi-level parallelism from laptops to supercomputers. *SoftwareX, 1-2*, 19-25.

Adler, E. (1977). Lignin chemistry—past, present and future. *Wood Science and Technology, 11*(3), 169-218.

Al Ameri, M. (2017). *Deep eutectic solvent pretreatment for enhancing biochemical conversion of switchgrass.* (M.S.). University of Missouri-Columbia,

Alvarez-Vasco, C., Ma, R., Quintero, M., Guo, M., Geleynse, S., Ramasamy, K. K., Wolcott, M., & Zhang, X. (2016). Unique low-molecular-weight lignin with high purity extracted from wood by deep eutectic solvents (DES): a source of lignin for valorization. *Green Chemistry, 18*(19), 5133-5141.

Besombes, S., & Mazeau, K. (2005a). The cellulose/lignin assembly assessed by molecular modeling. Part 1: adsorption of a threo guaiacyl β-O-4 dimer onto a Iβ cellulose whisker. *Plant Physiology and Biochemistry, 43*(3), 299-308.

Besombes, S., & Mazeau, K. (2005b). The cellulose/lignin assembly assessed by molecular modeling. Part 2: Seeking for evidence of organization of lignin molecules at the interface with cellulose. *Plant Physiology and Biochemistry, 43*(3), 277-286.

BIOVIA, D. S. (2011). Material Studio 6.0. *San Diego: Dassault Systèmes*.

Boerjan, W., Ralph, J., & Baucher, M. (2003). Lignin biosynthesis. *Annual Review of Plant Biology, 54*(1), 519-546.

Brehm, M., & Kirchner, B. (2011). TRAVIS-a free analyzer and visualizer for Monte Carlo and molecular dynamics trajectories. *Journal of Chemical Information and Modeling, 51*(8), 2007-2023.

Chen, Y., Zhang, L., Yu, J., Lu, Y., Jiang, B., Fan, Y., & Wang, Z. (2019). High-purity lignin isolated from poplar wood meal through dissolving treatment with deep eutectic solvents. *Royal Society Open Science, 6*(1), 181757.

Chen, Z., Bai, X., A, L., & Wan, C. (2018a). High-Solid Lignocellulose Processing Enabled by Natural Deep Eutectic Solvent for Lignin Extraction and Industrially

Relevant Production of Renewable Chemicals. *ACS Sustainable Chemistry & Engineering, 6*(9), 12205-12216.

Chen, Z., Bai, X., A, L., Zhang, H., & Wan, C. (2020). Insights into Structural Changes of Lignin toward Tailored Properties during Deep Eutectic Solvent Pretreatment. *ACS Sustainable Chemistry & Engineering, 8*(26), 9783-9793.

Chen, Z., Bai, X., & Wan, C. (2018b). High-solid lignocellulose processing enabled by natural deep eutectic solvent for lignin extraction and industrially relevant production of renewable chemicals. *ACS Sustainable Chemistry & Engineering, 6*(9), 12205-12216.

Chen, Z., Ragauskas, A., & Wan, C. (2020). Lignin extraction and upgrading using deep eutectic solvents. *Industrial Crops and Products, 147*, 112241-112241.

Chen, Z., Reznicek, W. D., & Wan, C. (2018c). Aqueous Choline Chloride: A Novel Solvent for Switchgrass Fractionation and Subsequent Hemicellulose Conversion into Furfural. *ACS Sustainable Chemistry & Engineering, 6*(5), 6910-6919.

Chen, Z., Sun, Y., & Wan, C. (2019). Effects of alkaline hydrogen peroxide treatment on cellulose accessibility of switchgrass pretreated by acidic deep eutectic solvent. *Cellulose, 26*(18), 9439-9446.

Chen, Z., & Wan, C. (2018). Ultrafast fractionation of lignocellulosic biomass by microwave-assisted deep eutectic solvent pretreatment. *Bioresource Technology, 250*, 532-537.

Chio, C., Sain, M., & Qin, W. (2019). Lignin utilization: A review of lignin depolymerization from various aspects. *Renewable and Sustainable Energy Reviews, 107*, 232-249.

D'Agostino, C., Harris, R. C., Abbott, A. P., Gladden, L. F., & Mantle, M. D. (2011). Molecular motion and ion diffusion in choline chloride based deep eutectic solvents studied by 1H pulsed field gradient NMR spectroscopy. *Physical Chemistry Chemical Physics, 13*(48), 21383-21391.

Doherty, B., & Acevedo, O. (2018). OPLS Force Field for Choline Chloride-Based Deep Eutectic Solvents. *The Journal of Physical Chemistry B, 122*(43), 9982-9993.

Francisco, M., van den Bruinhorst, A., Zubeir, L. F., Peters, C. J., & Kroon, M. C. (2013). A new low transition temperature mixture (LTTM) formed by choline chloride+lactic acid: Characterization as solvent for CO2 capture. *Fluid Phase Equilibria, 340*, 77-84.

Frauenkron, M., Melder, J.-P., Ruider, G., Rossbacher, R., & Höke, H. (2012). Ethanolamines and propanolamines. *Environmental Protection, 421*, 8.

Freudenberg, K., & Neish, A. C. (1968). *Constitution and biosynthesis of lignin*. Berlin: Springer-Verlag.

García, A., Toledano, A., Andrés, M. Á., & Labidi, J. (2010). Study of the antioxidant capacity of Miscanthus sinensis lignins. *Process Biochemistry, 45*(6), 935-940.

García, G., Atilhan, M., & Aparicio, S. (2015). The impact of charges in force field parameterization for molecular dynamics simulations of deep eutectic solvents. *Journal of Molecular Liquids, 211*, 506-514.

George, A., Tran, K., Morgan, T. J., Benke, P. I., Berrueco, C., Lorente, E., Wu, B. C., Keasling, J. D., Simmons, B. A., & Holmes, B. M. (2011). The effect of ionic liquid cation and anion combinations on the macromolecular structure of lignins. *Green Chemistry, 13*(12), 3375-3385.

Gilmore, M., Moura, L. M., Turner, A. H., Swadźba-Kwaśny, M., Callear, S. K., McCune, J. A., Scherman, O. A., & Holbrey, J. D. (2018). A comparison of choline:urea and choline:oxalic acid deep eutectic solvents at 338 K. *The Journal of Chemical Physics, 148*(19), 193823.

Guo, Z., Ling, Z., Wang, C., Zhang, X., & Xu, F. (2018). Integration of facile deep eutectic solvents pretreatment for enhanced enzymatic hydrolysis and lignin valorization from industrial xylose residue. *Bioresource Technology, 265*, 334-339.

Halgren, T. A. (1996). Merck molecular force field. I. Basis, form, scope, parameterization, and performance of MMFF94. *Journal of Computational Chemistry, 17*(5-6), 490-519.

Hamelinck, C. N., Hooijdonk, G. V., & Faaij, A. P. C. (2005). Ethanol from lignocellulosic biomass: techno-economic performance in short-, middle-and long-term. *Biomass and Bioenergy, 28*(4), 384-410.

Hammond, K. D., Naeger, I. V., Widanagamaachchi, W., Lo, L.-T., Maroudas, D., & Wirth, B. D. (2019). Helium flux effects on bubble growth and surface morphology in plasma-facing tungsten from large-scale molecular dynamics simulations. *Nuclear Fusion, 59*(6), 066035.

Hammond, O. S., Bowron, D. T., & Edler, K. J. (2016). Liquid structure of the choline chloride-urea deep eutectic solvent (reline) from neutron diffraction and atomistic modelling. *Green Chemistry, 18*(9), 2736-2744.

Harifi-Mood, A. R., & Buchner, R. (2017). Density, viscosity, and conductivity of choline chloride + ethylene glycol as a deep eutectic solvent and its binary mixtures with dimethyl sulfoxide. *Journal of Molecular Liquids, 225*, 689-695.

Hou, X.-D., Li, A.-L., Lin, K.-P., Wang, Y.-Y., Kuang, Z.-Y., & Cao, S.-L. (2018). Insight into the structure-function relationships of deep eutectic solvents during rice straw pretreatment. *Bioresource Technology, 249*, 261-267.

Houtman, C. J., & Atalla, R. H. (1995). Cellulose-lignin interactions (a computational study). *Plant Physiology, 107*(3), 977-984.

Humphrey, W., Dalke, A., & Schulten, K. (1996). VMD: visual molecular dynamics. *Journal of Molecular Graphics, 14*(1), 33-38.

Janesko, B. G. (2011). Modeling interactions between lignocellulose and ionic liquids using DFT-D. *Physical Chemistry Chemical Physics, 13*(23), 11393-11401.

Jewett, A. I., Zhuang, Z., & Shea, J.-E. (2013). Moltemplate a coarse-grained model assembly tool. *Biophysical Journal, 104*(2), 169-169.

Ji, H., & Lv, P. (2020). Mechanistic insights into the lignin dissolution behaviors of a recyclable acid hydrotrope, deep eutectic solvent (DES), and ionic liquid (IL). *Green Chemistry, 22*(4), 1378-1387.

Ji, W., Ding, Z., Liu, J., Song, Q., Xia, X., Gao, H., Wang, H., & Gu, W. (2012). Mechanism of Lignin Dissolution and Regeneration in Ionic Liquid. *Energy & Fuels, 26*(10), 6393-6403.

Jia, S., Cox, B. J., Guo, X., Zhang, Z. C., & Ekerdt, J. G. (2011). Hydrolytic Cleavage of β-O-4 Ether Bonds of Lignin Model Compounds in an Ionic Liquid with Metal Chlorides. *Industrial & Engineering Chemistry Research, 50*(2), 849-855.

Jorgensen, W., Maxwell, D. S., & Tirado-Rives, J. (1996). Development and testing of the OPLS all-atom force field on conformational energetics and properties of organic liquids. *Journal of the American Chemical Society, 118*(45), 11225-11236.

Kirk, T. K., & Obst, J. R. (1988). Lignin determination. *Methods in Enzymology, 161*, 87-101.

Kumar, A. K., Parikh, B. S., & Pravakar, M. (2016). Natural deep eutectic solvent mediated pretreatment of rice straw: bioanalytical characterization of lignin extract and enzymatic hydrolysis of pretreated biomass residue. *Environmental Science and Pollution Research, 23*(10), 9265-9275.

Larsson, P. T., Hult, E.-L., Wickholm, K., Pettersson, E., & Iversen, T. (1999). CP/MAS 13C-NMR spectroscopy applied to structure and interaction studies on cellulose I. *Solid State Nuclear Magnetic Resonance, 15*(1), 31-40.

Leron, R. B., Soriano, A. N., & Li, M.-H. (2012). Densities and refractive indices of the deep eutectic solvents (choline chloride+ ethylene glycol or glycerol) and their

aqueous mixtures at the temperature ranging from 298.15 to 333.15 K. *Journal of the Taiwan Institute of Chemical Engineers, 43*(4), 551-557.

Li, A.-L., Hou, X.-D., Lin, K.-P., Zhang, X., & Fu, M.-H. (2018). Rice straw pretreatment using deep eutectic solvents with different constituents molar ratios: Biomass fractionation, polysaccharides enzymatic digestion and solvent reuse. *Journal of Bioscience and Bioengineering, 126*(3), 346-354.

Li, T., Lyu, G., Liu, Y., Lou, R., Lucia, L. A., Yang, G., Chen, J., & Saeed, H. A. (2017). Deep Eutectic Solvents (DESs) for the Isolation of Willow Lignin (Salix matsudana cv. Zhuliu). *International Journal of Molecular Sciences, 18*(11), 2266.

Lindner, B., Petridis, L., Schulz, R., & Smith, J. C. (2013). Solvent-driven preferential association of lignin with regions of crystalline cellulose in molecular dynamics simulation. *Biomacromolecules, 14*(10), 3390-3398.

Liu, C.-G., Xiao, Y., Xia, X.-X., Zhao, X.-Q., Peng, L., Srinophakun, P., & Bai, F.-W. (2019). Cellulosic ethanol production: Progress, challenges and strategies for solutions. *Biotechnology Advances, 37*(3), 491-504.

Liu, Q., Wang, S., Zheng, Y., Luo, Z., & Cen, K. (2008). Mechanism study of wood lignin pyrolysis by using TG-FTIR analysis. *Journal of Analytical and Applied Pyrolysis, 82*(1), 170-177.

Liu, Q., Zhao, X., Yu, D., Yu, H., Zhang, Y., Xue, Z., & Mu, T. (2019). Novel deep eutectic solvents with different functional groups towards highly efficient dissolution of lignin. *Green Chemistry, 21*(19), 5291-5297.

Liu, Y., Chen, W., Xia, Q., Guo, B., Wang, Q., Liu, S., Liu, Y., Li, J., & Yu, H. (2017). Efficient Cleavage of Lignin-Carbohydrate Complexes and Ultrafast Extraction of Lignin Oligomers from Wood Biomass by Microwave-Assisted Treatment with Deep Eutectic Solvent. *ChemSusChem, 10*(8), 1692-1700.

Losada, M., Tran, H., & Xu, Y. (2008). Lactic acid in solution: investigations of lactic acid self-aggregation and hydrogen bonding interactions with water and methanol using vibrational absorption and vibrational circular dichroism spectroscopies. *The Journal of Chemical Physics, 128*(1), 014508.

Lynam, J. G., Kumar, N., & Wong, M. J. (2017). Deep eutectic solvents' ability to solubilize lignin, cellulose, and hemicellulose; thermal stability; and density. *Bioresource Technology, 238*, 684-689.

Lyu, G., Li, T., Ji, X., Yang, G., Liu, Y., Lucia, L. A., & Chen, J. (2018). Characterization of Lignin Extracted from Willow by Deep Eutectic Solvent Treatments. *Polymers, 10*(8), 869-869.

Mainberger, S., Kindlein, M., Bezold, F., Elts, E., Minceva, M., & Briesen, H. (2017). Deep eutectic solvent formation: a structural view using molecular dynamics simulations with classical force fields. *Molecular Physics, 115*(9-12), 1309-1321.

Moyer, P., Smith, M. D., Abdoulmoumine, N., Chmely, S. C., Smith, J. C., Petridis, L., & Labbé, N. (2018). Relationship between lignocellulosic biomass dissolution and physicochemical properties of ionic liquids composed of 3-methylimidazolium cations and carboxylate anions. *Physical Chemistry Chemical Physics, 20*(4), 2508-2516.

Muley, P. D., Mobley, J. K., Tong, X., Novak, B., Stevens, J., Moldovan, D., Shi, J., & Boldor, D. (2019). Rapid microwave-assisted biomass delignification and lignin depolymerization in deep eutectic solvents. *Energy Conversion and Management, 196*, 1080-1088.

Perkins, S. L., Painter, P., & Colina, C. M. (2013). Molecular Dynamic Simulations and Vibrational Analysis of an Ionic Liquid Analogue. *The Journal of Physical Chemistry B, 117*(35), 10250-10260.

Perkins, S. L., Painter, P., & Colina, C. M. (2014). Experimental and Computational Studies of Choline Chloride-Based Deep Eutectic Solvents. *Journal of Chemical & Engineering Data, 59*(11), 3652-3662.

Plimpton, S. (1995). Fast parallel algorithms for short-range molecular dynamics. *Journal of Computational Physics, 117*, 1-19.

Procentese, A., Johnson, E., Orr, V., Garruto Campanile, A., Wood, J. A., Marzocchella, A., & Rehmann, M. L. (2015). Deep eutectic solvent pretreatment and subsequent saccharification of corncob. *Bioresource Technology, 192*, 31-36.

Procentese, A., Raganati, F., Olivieri, G., Russo, M. E., Rehmann, L., & Marzocchella, A. (2017). Low-energy biomass pretreatment with deep eutectic solvents for bio-butanol production. *Bioresource Technology, 243*, 464-473.

Procentese, A., Raganati, F., Olivieri, G., Russo, M. E., Rehmann, L., & Marzocchella, A. (2018). Deep Eutectic Solvents pretreatment of agro-industrial food waste. *Biotechnology for Biofuels, 11*, 37.

Remsing, R. C., Swatloski, R. P., Rogers, R. D., & Moyna, G. (2006). Mechanism of cellulose dissolution in the ionic liquid 1-n-butyl-3-methylimidazolium chloride: a 13 C and 35/37 Cl NMR relaxation study on model systems. *Chemical Communications*(12), 1271-1273.

Rismiller, S. C., Groves, M. M., Meng, M., Dong, Y., & Lin, J. (2018). Water assisted liquefaction of lignocellulose biomass by ReaxFF based molecular dynamic simulations. *Fuel, 215*, 835-843.

Rogner, H., Aguilera, R. F., Archer, C., Bertani, R., Bhattacharya, S., Dusseault, M., Gagnon, L., Harbel, H., Hoogwijk, M., Johnson, A., Rogner, M., Wagner, H., & Yakushev, V. (2012). Energy resources and potentials. In T. B. Johansson, A. Patwardhan, N. Nakicenovic, & L. Gomez-Echeverri (Eds.), *Global Energy Assessment: Toward a Sustainable Future* (pp. 423-512). USA: Cambridge University Press.

Sanderson, M., Reed, R., McLaughlin, S., Wullschleger, S., Conger, B., Parrish, D., Wolf, D., Taliaferro, C., Hopkins, A., & Ocumpaugh, W. (1996). Switchgrass as a sustainable bioenergy crop. *Bioresource Technology, 56*(1), 83-93.

Sankaran, R., Parra Cruz, R. A., Pakalapati, H., Show, P. L., Ling, T. C., Chen, W.-H., & Tao, Y. (2020). Recent advances in the pretreatment of microalgal and lignocellulosic biomass: A comprehensive review. *Bioresource Technology, 298*, 122476.

Santos, A. C. d., Ximenes, E., Kim, Y., & Ladisch, M. R. (2019). Lignin-enzyme interactions in the hydrolysis of lignocellulosic biomass. *Trends in Biotechnology, 37*(5), 518-531.

Shah, D., & Mjalli, F. S. (2014). Effect of water on the thermo-physical properties of Reline: An experimental and molecular simulation based approach. *Physical Chemistry Chemical Physics, 16*(43), 23900-23907.

Smink, D., Juan, A., Schuur, B., & Kersten, S. R. A. (2019). Understanding the Role of Choline Chloride in Deep Eutectic Solvents Used for Biomass Delignification. *Industrial & Engineering Chemistry Research, 58*(36), 16348-16357.

Smith, E. L., Abbott, A. P., & Ryder, K. S. (2014). Deep eutectic solvents (DESs) and their applications. *Chemical Reviews, 114*(21), 11060-11082.

Smith, M. D., Mostofian, B., Cheng, X., Petridis, L., Cai, C. M., Wyman, C. E., & Smith, J. C. (2016). Cosolvent pretreatment in cellulosic biofuel production: effect of tetrahydrofuran-water on lignin structure and dynamics. *Green Chemistry, 18*(5), 1268-1277.

Soares, B., Tavares, D. J. P., Amaral, J. L., Silvestre, A. J. D., Freire, C. S. R., & Coutinho, J. A. P. (2017). Enhanced solubility of lignin monomeric model compounds and technical lignins in aqueous solutions of deep eutectic solvents. *ACS Sustainable Chemistry & Engineering, 5*(5), 4056-4065.

Sun, H., Li, Y., Wu, X., & Li, G. (2013). Theoretical study on the structures and properties of mixtures of urea and choline chloride. *Journal of Molecular Modeling, 19*(6), 2433-2441.

Tan, Y. T., Ngoh, G. C., & Chua, A. S. M. (2019). Effect of functional groups in acid constituent of deep eutectic solvent for extraction of reactive lignin. *Bioresource Technology, 281*, 359-366.

Thakur, V. K., Thakur, M. K., Raghavan, P., & Kessler, M. R. (2014). Progress in green polymer composites from lignin for multifunctional applications: a review. *ACS Sustainable Chemistry & Engineering, 2*(5), 1072-1092.

van Osch, D. J., Kollau, L. J., van den Bruinhorst, A., Asikainen, S., Rocha, M. A., & Kroon, M. C. (2017). Ionic liquids and deep eutectic solvents for lignocellulosic biomass fractionation. *Physical Chemistry Chemical Physics, 19*(4), 2636-2665.

Vermaas, J. V., Crowley, M. F., & Beckham, G. T. (2019). A Quantitative Molecular Atlas for Interactions Between Lignin and Cellulose. *ACS Sustainable Chemistry & Engineering, 7*(24), 19570-19583.

Wang, H., Jia, Y., Wang, X., Yao, Y., Yue, D., & Jing, Y. (2013). Electrochemical deposition of magnesium from analogous ionic liquid based on dimethylformamide. *Electrochimica Acta, 108*, 384-389.

Wang, J., Wolf, R. M., Caldwell, J. W., Kollman, P. A., & Case, D. A. (2004). Development and testing of a general amber force field. *Journal of Computational Chemistry, 25*(9), 1157-1174.

Wang, Z.-K., Hong, S., Wen, J.-l., Ma, C.-Y., Tang, L., Jiang, H., Chen, J.-J., Li, S., Shen, X.-J., & Yuan, T.-Q. (2019). Lewis Acid-Facilitated Deep Eutectic Solvent (DES) Pretreatment for Producing High-Purity and Antioxidative Lignin. *ACS Sustainable Chemistry & Engineering, 8*(2), 1050-1057.

Wen, J.-L., Yuan, T.-Q., Sun, S.-L., Xu, F., & Sun, R.-C. (2014). Understanding the chemical transformations of lignin during ionic liquid pretreatment. *Green Chemistry, 16*(1), 181-190.

Wyman, C. E., Cai, C. M., & Kumar, R. (2017). Bioethanol from Lignocellulosic Biomass. In R. A. Meyers (Ed.), *Encyclopedia of Sustainability Science and Technology* (pp. 1-27). New York, NY: Springer New York.

Xia, Q., Liu, Y., Meng, J., Cheng, W., Chen, W., Liu, S., Liu, Y., Li, J., & Yu, H. (2018). Multiple hydrogen bond coordination in three-constituent deep eutectic solvents enhances lignin fractionation from biomass. *Green Chemistry, 20*(12), 2711-2721.

Xu, C., Wu, Q., Hua, Y., & Li, J. (2014). The electrodeposition of Zn-Ti alloys from ZnCl 2-urea deep eutectic solvent. *Journal of Solid State Electrochemistry, 18*(8), 2149-2155.

Xu, H., Kong, Y., Peng, J., Song, X., Liu, Y., Su, Z., Li, B., Gao, C., & Tian, W. (2021). Comprehensive analysis of important parameters of choline chloride-based deep

eutectic solvent pretreatment of lignocellulosic biomass. *Bioresource Technology, 319*, 124209.

Yu, Z., Tu, J., Wang, C., & Jiao, S. (2019). A Rechargeable Al/Graphite Battery Based on AlCl3/1-butyl-3-methylimidazolium Chloride Ionic Liquid Electrolyte. *ChemistrySelect, 4*(11), 3018-3024.

Zahn, S., Kirchner, B., & Mollenhauer, D. (2016). Charge Spreading in Deep Eutectic Solvents. *ChemPhysChem, 17*(21), 3354-3358.

Zakzeski, J., Bruijnincx, P. C. A., Jongerius, A. L., & Weckhuysen, B. M. (2010). The Catalytic Valorization of Lignin for the Production of Renewable Chemicals. *Chemical Reviews, 110*(6), 3552-3599.

Zdanowicz, M., Wilpiszewska, K., & Spychaj, T. (2018). Deep eutectic solvents for polysaccharides processing. A review. *Carbohydrate Polymers, 200*, 361-380.

Zhang, T., Li, X., & Guo, L. (2017). Initial Reactivity of Linkages and Monomer Rings in Lignin Pyrolysis Revealed by ReaxFF Molecular Dynamics. *Langmuir, 33*(42), 11646-11657.

Zhang, T., Li, X., Qiao, X., Zheng, M., Guo, L., Song, W., & Lin, W. (2016). Initial Mechanisms for an Overall Behavior of Lignin Pyrolysis through Large-Scale ReaxFF Molecular Dynamics Simulations. *Energy & Fuels, 30*(4), 3140-3150.

Zhang, Y., He, H., Dong, K., Fan, M., & Zhang, S. (2017). A DFT study on lignin dissolution in imidazolium-based ionic liquids. *RSC Advances, 7*(21), 12670-12681.

Zhang, Y., Huo, F., Wang, Y., Xia, Y., Tan, X., Zhang, S., & He, H. (2019). Theoretical Elucidation of β-O-4 Bond Cleavage of Lignin Model Compound Promoted by Sulfonic Acid-Functionalized Ionic Liquid. *Frontiers in Chemistry, 7*, 78.

Zhekenov, T., Toksanbayev, N., Kazakbayeva, Z., Shah, D., & Mjalli, F. S. (2017). Formation of type III Deep Eutectic Solvents and effect of water on their intermolecular interactions. *Fluid Phase Equilibria, 441*, 43-48.

Zhu, Y., Yan, J., Liu, C., & Zhang, D. (2017). Modeling interactions between a β-O-4 type lignin model compound and 1-allyl-3-methylimidazolium chloride ionic liquid. *Biopolymers, 107*(8), e23022.

Zubeltzu, J., Formoso, E., & Rezabal, E. (2020). Lignin solvation by ionic liquids: The role of cation. *Journal of Molecular Liquids, 303*, 112588.